CIRCULATION COPY
SUBJECT TO RECALL
IN TWO WEEKS

UCRL- 93395
PREPRINT

# INTERCHANGE, ROTATIONAL, AND BALLOONING STABILITY OF LONG-THIN AXISYMMETRIC SYSTEMS WITH FINITE ORBIT EFFECTS

Bruce I. Cohen
Robert P. Freis
William A. Newcomb

This paper was prepared for submittal to
PHYSICS OF FLUIDS

September 19, 1985

Lawrence
Livermore
National
Laboratory

This is a preprint of a paper intended for publication in a journal or proceedings. Since changes may be made before publication, this preprint is made available with the understanding that it will not be cited or reproduced without the permission of the author.

# DISCLAIMER

This document was prepared as an account of work sponsored by an agency of the United States Government. Neither the United States Government nor the University of California nor any of their employees, makes any warranty, express or implied, or assumes any legal liability or responsibility for the accuracy, completeness, or usefulness of any information, apparatus, product, or process disclosed, or represents that its use would not infringe privately owned rights. Reference herein to any specific commercial products, process, or service by trade name, trademark, manufacturer, or otherwise, does not necessarily constitute or imply its endorsement, recommendation, or favoring by the United States Government or the University of California. The views and opinions of authors expressed herein do not necessarily state or reflect those of the United States Government or the University of California, and shall not be used for advertising or product endorsement purposes.

# INTERCHANGE, ROTATIONAL, AND BALLOONING STABILITY OF LONG-THIN AXISYMMETRIC SYSTEMS WITH FINITE ORBIT EFFECTS*

Bruce I. Cohen, Robert P. Freis, and William A. Newcomb
Lawrence Livermore National Laboratory, University of California
Livermore, California 94550

## ABSTRACT

The stability of axisymmetric tandem mirror plasmas with respect to interchange, rotational, and ballooning modes is investigated in the paraxial approximation. The stabilizing effects of finite orbits, energetic fast-drifting electrons, nearby conducting walls, and line-tying by a cold plasma halo are incorporated. The FLORA computer code is introduced to perform calculations of equilibria with finite plasma pressure and to determine linear stability by integrating a two-dimensional initial-value equation. Numerical calculations with FLORA support and extend analytical results. Analytical and numerical stability criteria are obtained.

## I. INTRODUCTION

This paper is concerned with the magnetohydrodynamic stability of plasmas in axisymmetric tandem mirror systems. The tandem mirror configuration is currently one of the two principal magnetic confinement approaches to controlled fusion.[1] The central cells of tandems are axisymmetric and much longer than the end cells or plugs that typically have quadrupole magnetic coils to ensure macroscopic stability.[1,2] These end cells are minimum-B structures whose good magnetic-field-line curvature offsets the bad curvature originating from elsewhere in the tandem mirror. Unfortunately, the quadrupole magnetic structure is both deleterious to radial transport,[3] which would be greatly improved in a completely axisymmetric system, and much more costly than are axisymmetric configurations. This motivates investigation of an axisymmetric tandem mirror as a possible confinement system. The assessment of its viability begins with calculations of equilibria with finite plasma pressure and an analysis of macroscopic stability as presented here. These calculations also provide further insight into the equilibrium and stability of long-thin tandem mirror systems with symmetric central cells in general.

One of the earliest considerations of the macroscopic stability of plasmas confined by magnetic fields from the point of view of particle orbits is the classic paper by Rosenbluth and Longmire.[4] This paper presented a physical picture of interchange stability and stated flute-mode stability criteria for a low-pressure plasma based on energy arguments. Magnetohydrodynamic (MHD) stability conditions were derived from the collisionless

Boltzmann equation in a slightly earlier paper.[5] Of direct importance to the study presented here was the development of finite-Larmor-radius (FLR) theory in Ref. 6. In this paper the Vlasov equation was formally expanded in the limits of small but finite Larmor radius, weak density gradient, low frequency relative to the cyclotron frequencies, and very low beta (beta is the ratio of the plasma pressure to the magnetic energy density). Gravity was used to model magnetic curvature; plasma equilibria and perturbations were uniform in z. A Gaussian density profile and rigid rotation were presumed. Because of their finite Larmor radius, the ions sample a different perturbed electric field than do the electrons sharing the same guiding center position. The associated charge separation is stabilizing when $(k_\perp a_i)^2 > \gamma/\omega_{ci}$, where $k_\perp$ is the perpendicular wavenumber of the interchange mode, $a_i$ is the ion Larmor radius, $\gamma$ is the ideal hydromagnetic growth rate, and $\omega_{ci}$ is the cyclotron frequency.[6] An important result of Ref. 6 was the lack of FLR stabilization for an m = 1 rigid shift of a cylindrical plasma (m is the azimuthal Fourier mode number). This suggests that the m = 1 mode may be the most difficult to stabilize in general.

The papers that have followed Ref. 6 have significantly refined the FLR theory of MHD equilibrium and stability. Roberts and Taylor obtained equations and results that were similar to Ref. 6 by an alternative derivation.[7] An improved derivation of the FLR equations was presented in Ref. 8. The authors of Ref. 8 considered general radial profiles, introduced a variational principle, and obtained a sufficient condition for stability. In Ref. 9 FLR equations were derived from the Vlasov equation, and an alternative derivation of Ref. 8's results was provided. Reference 10 extended the calculations of

Ref. 8 to finite beta slab systems with gravity and no z variations. A stability analysis similar to that in Ref. 10 was applied in Ref. 11 to a finite-beta, rotating straight $\theta$ pinch, which included a z variation of the perturbed motion parallel to the magnetic field and featured a numerical solution of a radial eigenequation. The $m = 1$ mode was determined not to be a rigid displacement in a diffuse-boundary plasma separated from a perfectly conducting wall by a vacuum region, and the rotational instabiity benefitted from FLR stabilization even for $m = 1$.

References 12-14 addressed both FLR effects and the MHD equilibrium and stability properties of systems with large aspect ratio.[12-14] Reference 12 applies Hamiltonian methods to the theory of MHD equilibrium and stability for rotating systems with no axial equilibrium variation. The axial variations of perturbed quantities are Fourier analyzed. An energy principal and a radial eigenequation are derived in Ref. 12. A similar Lagrangian formulation of the MHD equations was published in Ref. 15. Reference 13 extends the methods of Ref. 12 to systems with FLR. An FLR Lagrangian is introduced from which Euler-Lagrange equations are calculated that agree with equations derived from the FLR expansion of the Vlasov equation. A potential energy is derived from which a sufficient condition for stability is obtained. This Lagrangian method was applied to the analysis of the equilibrium and stability of large aspect-ratio systems neglecting FLR in Ref. 14. Three-dimensional systems were examined in the paraxial or long-thin limit, which is appropriate to many single-cell and tandem mirror systems. A good review of three-dimensional MHD equilibrium and stability issues in mirror plasmas was provided in Sec. 2.2 of Ref. 2.

Particularly important contributions to the theoretical foundation for the present work are found in Refs. 16-18. The Vlasov equation was expanded once again using the FLR ordering scheme, and moment equations were calculated to obtain a radial differential dispersion equation in which the effects of line bending and field-line curvature in a finite-beta screw-pinch configuration were additive to the FLR effects. A compact heuristic derivation of the stability equation accompanies the rigorous derivation in Ref. 18. The important point is that the MHD geometrical effects of line bending and curvature are simply additive to the FLR effects because they are separately small in their respective expansion parameters, the paraxial parameter $\lambda = R/L << 1$ and the FLR parameter $\nu \equiv a/R << 1$, where R and L are the radial and axial scale lengths and a is the Larmor radius. This has been confirmed for systems with three-dimensional equilibrium variation.[19]

There have been a number of recent MHD stability studies for tandem mirror systems. References 20 and 21 used gyrokinetic theory to calculate tandem mirror stability with finite-orbit modifications in eikonal and paraxial limits at finite beta for anisotropic pressure and three-dimensional equilibria. They obtained ballooning-mode equations and found wave-particle-resonance and trapped-particle effects were higher order in the paraxial parameter than were curvature drive and line bending. FLR effects were determined to be strongly stabilizing and enhanced because of their influence over the entire length of the tandem mirror in contrast to curvature effects that typically are severely destabilizing only over a limited domain. References 22 and 23 provide numerical solutions of the high-m paraxial ballooning equation with and without FLR effects and with the perturbed displacement line-tied at some axial position to model the stabilizing end plugs of the tandem mirror. These calculations determined the critical central-cell beta at marginal stability as functions of the FLR magnitude and the line-tying positions. Numerical solutions of the low-m paraxial ballooning equation with no FLR effects to determine the stability of a tandem mirror with a sharp-boundary radial profile are reported in Ref. 24. Reference 25 considered the high-m paraxial ballooning equation with no FLR effects for an axisymmetric tandem mirror stabilized by energetic electrons in the end plugs. The energetic electrons were rigid with respect to the MHD perturbations in this model, and there was an examination of the validity of the line-tying model employed in Refs. 22-24.

There also have been numerical calculations of the ballooning stability of tandem mirrors incorporating the detailed structure of the quadrupole end plugs used in current experiments. Numerical calculations of high-m, paraxial ballooning stability for the TMX-U and MFTF-B tandem mirror experiments at Lawrence Livermore National Laboratory were reported in Ref. 26. The same equilibrium and stability code (TEBASCO) has addressed m = 1, radially rigid ballooning stability in quadrupole tandem mirrors.[27] The assumption of rigidity in the radial eigenmode profile, motivated by FLR considerations, allows the reduction to a one-dimensional paraxial ballooning equation, which is then solved numerically in TEBASCO with a shooting method. Reference 28 presented a study of low-m ballooning and rotational modes with FLR effects in low-beta quadrupole tandems. A Galerkin method was used to construct three-dimensional eigenfunctions and to solve for the complex eigenfrequencies from the resulting characteristic polynomial. The variational principle in Ref. 28

was based on the Lagrangian formulation of MHD stability with FLR in a paraxial system presented in Refs. 12-14, and 19 and was applied to calculation of the low-m stability of the University of Wisconsin Phaedrus tandem mirror experiment. A similar stability calculation employing a paraxial variational principle and trial functions applied to quadrupole tandem mirrors was presented in an earlier publication.[29]

The calculations presented here address interchange, rotational, and ballooning instabilities for arbitrary values of m in axisymmetric tandem mirrors with FLR effects. The configurations are presumed to be long and thin, and the plasma beta can be finite. We obtain a linearized equation of motion for the flux tube displacement from the FLR Lagrangian for a paraxial system. The formal derivation of the Lagrangian has been given in Refs. 12, 14, and 19. The focus of this paper is the general numerical and specific analytical solution of the linear equation of motion and applications to tandem mirror stability.

One of our principal contributions is the introduction of the FLORA computer code to perform the numerical integration of the linearized equation of motion, which is solved as a two-dimensional initial-value problem. FLORA computes the radial and axial structure of the eigenfunctions using the magnetic flux $\psi$ and axial position z along the field line as independent spatial variables. The code accommodates a variety of radial and axial profiles for the density, pressure, vacuum magnetic field, and FLR coefficients. Perpendicular and parallel pressure balances relate the pressure components and determine the self-consistent magnetic field; this constitutes the equilibrium computations in FLORA that precede the stability calculations. Numerical and analytical results illustrate various types of low-frequency MHD instabilities in axisymmetric systems and the stabilizing influences of FLR, nearby conducting walls, line-tying by cold plasma halos, and energetic electrons.

The remaining contents of this paper are organized as follows, Sec. II sketches the Lagrangian theory of MHD stability. The basic assumptions and equilibrium relations for paraxial systems are presented here, and the linear and nonlinear equations of motion for incompressible displacements of the flux tubes are derived from Euler-Lagrange equations. We also construct a conserved energy for the linearly perturbed system, which provides a sufficient condition for stability. Section III describes our numerical integration of the linear equation of motion in the FLORA computer code. Several model problems are presented in Sec. IV; these examples either admit analytical solutions for the linear equation of motion or in one case have been solved numerically in an earlier study. They provide both valuable insight and thorough tests of FLORA. We model the paraxial equilibria of axisymmetric tandem mirrors in Sec. V. We examine the stabilizing influence of energetic electrons that are mirror-confined in the end cells of a tandem mirror in Sec. VI. The electrons dig a stabilizing magnetic well for the plasma and are presumed not to respond to MHD perturbations because of their rapid drifts. Section VII contains analytical and numerical studies of the MHD stabilization afforded by a cold plasma halo that line-ties the surface of an interchange-unstable hot-plasma core. The paper is concluded in Sec. VIII with a discussion that summarizes the paper's results and comments on research in progress and future directions.

## II. DERIVATION OF THE FIELD-LINE EQUATION OF MOTION

### A. Paraxial Equilibrium

The foundations for the equilibrium and stability theory presented here have been previously presented in Refs. 12-14, and 19. In this theory moments of the Vlasov equation are calculated in the limits of small inverse aspect ratio $\lambda = R/L \ll 1$ and small Larmor radius so that $\nu = a/R \ll 1$. These two expansion parameters are assumed to be comparable.

The magnetostatic equilibrium condition is

$$\underline{J} \times \underline{B} - \nabla \cdot \underline{\underline{P}} = 0 \tag{1}$$

for a charge-neutral system in rationalized emu units. The phase-space distribution functions are functions of the constants of the motion. We further specialize to axisymmetric equilibria. Hence, the components of the pressure tensor are functions of the magnetic field B and the magnetic flux $\psi$, but are independent of the angle variable; this is a condition of isorrhopy. One uses $\nabla \times \underline{B} = \underline{J}$ and $\underline{\underline{P}} = p_\perp(\underline{\underline{I}} - \hat{b}\hat{b}) + p_\parallel \hat{b}\hat{b}$ to reduce Eq. (1) to

$$\left[\nabla\left(\frac{B^2}{2} + p_\perp\right)\right]_\perp = rB\,\frac{\partial}{\partial\psi}\left(\frac{B^2}{2} + p_\perp\right) = 0 \tag{2}$$

to lowest order in $\lambda$ and $\nu$. This is a statement of perpendicular pressure balance and implies

$$\frac{B^2}{2} + p_\perp = P(z) \quad , \tag{3}$$

a function only of z. At first order in $\lambda$ and $\nu$, one obtains the parallel pressure balance condition

$$\hat{b} \cdot \nabla\left(\frac{B^2}{2} + p_\perp\right) - \underline{B} \cdot \nabla[(B^2 + p_\perp - p_\parallel)/B] = 0 \ . \tag{4}$$

All pressure components have been summed over species in Eqs. (1-4).

The curvature of the flux lines $\hat{b} \cdot \nabla \hat{b}$ is second order in $\lambda$. Thus, $\hat{b} \cdot \nabla = \partial/\partial z + \mathcal{O}(\lambda^2) \approx \partial/\partial z$. Furthermore, as a consequence of the paraxial approximation and $\nabla \cdot \underline{B} = 0$, $B_r$ is of order $\lambda$ compared to $B_z$; hence, $B^2 = B_z^2 + \mathcal{O}(\lambda^2)$. As yet, there have been no modifications due to FLR effects. These emerge at second order in $\nu$ when there are finite angular variations in the equilibrium or perturbed quantities.

Equations (2-4) are the plasma equilibrium conditions. We now review a number of constraints we choose to impose. These limit the arbitrariness of the distribution functions.[14,19] The constraints are most familiarly expressed in terms of the allowed dependences of $p_\perp$ and $p_\parallel$ on B and $\psi$.

We first assume that the phase-space distribution functions are functions of energy

$$\epsilon_s = m_s v_\parallel^2/2 + \mu B + q_s \phi \tag{5a}$$

and magnetic moment

$$\mu = m_s v^2/2B \tag{5b}$$

for each species s. The partial pressure components for the various species are

$$p_{\parallel s} = 4\pi B m_s \int \frac{d\mu d\varepsilon}{v_\parallel} v_\parallel^2 f_s \tag{6a}$$

and

$$p_{\perp s} = 4\pi B m_s \int \frac{d\mu d\varepsilon}{v_\parallel} \mu B f_s \ . \tag{6b}$$

In the absence of an ambipolar potential ($\phi = 0$), parallel pressure balance for each species is

$$p_{\perp s}(B) = - B^2 \frac{\partial}{\partial B}(p_{\parallel s}/B) \ . \tag{7}$$

With a finite ambipolar potential, Eq. (7) remains true only if summed over species and charge neutrality is assumed. (A sum over species is to be understood when the species subscript s is omitted). The pressure components and the number density are strictly nonnegative. Equation (7) becomes

$$p_{\perp s}(B) = - B^2 \frac{\partial}{\partial B} (\frac{p_{\parallel s}}{B}) - n_s q_s B \frac{\partial}{\partial B} \phi \tag{8}$$

when $\phi \neq 0$. The self-consistent ambipolar potential is determined by the quasineutrality condition. Realistic calculation of distribution functions and the self-consistent ambipolar potential requires a model for plasma transport, which is beyond the scope of this paper. Various ad hoc model potential profiles will be considered.

We next impose two macroscopic stability conditions that are related to the well-posedness of the equilibrium problem.[14] Stability with respect to the firehose mode (lengthwise buckling of the magnetic field lines) requires

$$Q \equiv B^2 + p_\perp - p_\parallel > 0 \ , \tag{9}$$

and with respect to the mirror mode,

$$B^2 \frac{\partial}{\partial B} \left(\frac{Q}{B}\right) > 0 \ . \tag{10}$$

Both these conditions will be assumed to be satisfied.

A sufficient condition for microstability often employed is that f be a monotone-decreasing function of energy

$$f_\varepsilon \leq 0 \ . \tag{11}$$

It then follows from Eqs. (6) and (11) that

$$\frac{\partial}{\partial B} \left(\frac{p_\perp}{B^2}\right) \leq 0 \ . \tag{12}$$

This remains true for a finite ambipolar potential.[14] However, Eq. (11) is a stronger stability condition than is necessary. Single-cell and tandem mirror plasmas are often stream-stabilized or stabilized with sloshing ions to prevent loss-cone instabilities. The associated stable distribution functions are frequently not monotone-decreasing functions of energy. Therefore, we shall not require conditions Eqs. (11) and (12) to be satisfied.

## B. FLR Lagrangian for Low-Frequency Motion

Curvature and FLR effects are found at second order in $\lambda$ and $\nu$ in the equations of motion. We also retain time derivatives at this order, which presupposes that all of the perturbed quantities have only low-frequency temporal variations. The FLR Lagrangian[13,14,19] is now introduced from which we derive the Euler-Lagrange equations describing the plasma and field-line motion in the plane transverse to $\underline{B}$ at second order in $\lambda$ and $\nu$ subject to the constraint of incompressibility. The Lagrangian density is

$$L = \frac{1}{2}(\rho\ |\underline{x}_t|^2 + \mathscr{X}\underline{x}_t \cdot \underline{x}_\theta - \mathscr{Y}|\underline{x}_\theta|^2 - Q\ |\underline{x}_z|^2)\ , \tag{13}$$

where $\underline{x} = (x,y)$ is the position of the magnetic field line expressed as a function of the flux coordinates $\psi$ and $\theta$, of the axial coordinate z, and of time t. The subscripts $\psi$, z, $\theta$, and t denote partial derivatives. The flux coordinates $\psi$ and $\theta$ have the property that

$$\underline{B} = \nabla\psi \times \nabla\theta\ . \tag{14}$$

We also require the definitions of the FLR coefficients[13,19]

$$\mathscr{X} = \rho(\Omega_1 + \Omega_2) = 2\rho\phi_\psi - \frac{(MB^2)_\psi}{2B} \tag{15a}$$

$$\mathscr{Y} = -\rho\Omega_1\Omega_2 = -\rho\phi_\psi^2 + (MB^2)_\psi \frac{\phi_\psi}{2B} - \frac{K_\psi B_\psi}{B} \tag{15b}$$

where

$$M = -\sum_s n_s m_s^2 \langle v_\perp^2\rangle_s / q_s B\ , \tag{16a}$$

$$K = -\sum_s n_s m_s^3 \langle v_\perp^4\rangle_s / 8q_s^2\ , \tag{16b}$$

$\rho$ is the mass density, $\phi$ is the ambipolar potential, $q_s$ is the species charge, $n_s$ is the species number density, $m_s$ is the species mass, and the bracket indicates an average over the distribution function. It should be noted that the quantity denoted as M has a simple physical interpretation as the density of gyrational angular momentum, and the quantity K is involved in the transport equation for M.[19]

For a rotating isothermal Maxwellian plasma,

$$\mathscr{X} = \sum_s \rho_s (2\Omega_E + \Omega_{\nabla B} + \Omega^*)_s \tag{17a}$$

and

$$\mathscr{Y} = -\sum_s \rho_s (\Omega_E + \Omega_{\nabla B})_s (\Omega_E + \Omega^*)_s \quad , \tag{17b}$$

where

$$\Omega_E = \partial\phi/\partial\psi \tag{18a}$$

$$\Omega^* = -\ (e_s n_s)^{-1}\ \partial p_{\perp s}/\partial\psi \tag{18b}$$

$$\Omega_{\nabla B} = (e_s n_s)^{-1}\ p_{\perp s}\partial \ell n B/\partial\psi \tag{18c}$$

are the azimuthal $\underline{E}\mathrm{x}\underline{B}$, diamagnetic, and $\nabla$B drift velocities.

In general, the coefficients $\rho$, $p_\perp$, $p_{||}$, $\mathscr{X}$, $\mathscr{Y}$, and Q are all functions of $\psi$ and z, and are independent of time. It can be shown that the Lagrangian (13) yields the same equation of motion as those calculated directly from moments of the Vlasov equation in the paraxial and small FLR approximations.[19]

An important constraint on the motion of the field lines is incompressibility. The Jacobian derived from Eq. (14) is

$$x_\psi y_\theta - x_\theta y_\psi = B^{-1} \tag{19}$$

and is maintained by the motion. Equations of motion can now be derived from an action principle with Eq. (19) incorporated as a constraint by introducing a Lagrange multiplier $\kappa = \kappa(\psi,\theta,z,t)$. The plasma is presumed to be tied to the field lines so that $(x_t, y_t)$ is the fluid velocity of both the plasma and the field lines. The boundary conditions on the perturbed transverse displacement are that it vanishes (shorted) on a lateral boundary surrounding the plasma, that it either vanishes or its axial derivative vanishes (insulated free-boundary condition) at the ends of the configuration, and that all quantities are periodic in $\theta$. The action is

$$I = \int_{t_1}^{t_2} dt \int dvol \; [L - \kappa(B\underline{x}_\psi \cdot \underline{x}_\theta^* - 1)] \quad , \tag{20}$$

where $\underline{x}^* \equiv \underline{x} \times \hat{b}$. We derive the Euler-Lagrange equations from $\delta I = 0$ by varying $\underline{x}$ along the trajectory, $\underline{x} \rightarrow \underline{x} + \underline{\delta x}$, with $\underline{\delta x} = 0$ at $t_1$ and $t_2$:

$$\delta I = \int_{t_1}^{t_2} dt \int d\psi dz d\theta \, \delta\underline{x}$$

$$\cdot \left[ -\frac{1}{B} \frac{\partial^2 L}{\partial t \partial \underline{x}_t} - \frac{\partial}{\partial \theta} \frac{1}{B} \frac{\partial L}{\partial \underline{x}} - \frac{\partial}{\partial z} \frac{1}{B} \frac{\partial L}{\partial \underline{x}_z} + \kappa_\theta \underline{x}_\psi^* - \kappa_\psi \underline{x}_\theta^* \right] = 0. \tag{21}$$

Because $\underline{\delta x}$ is arbitrary for $t \neq t_1, t_2$, then the expression in the square bracket must vanish for I to be stationary. One computes the scalar product of this with $\underline{x}_\psi$ and $\underline{x}_\theta$, and uses $\underline{x}_\theta \cdot \underline{x}_\psi^* = - \underline{x}_\theta^* \cdot \underline{x}_\psi = B^{-1}$ and $\underline{x}_\psi \cdot \underline{x}_\psi^* = \underline{x}_\theta \cdot \underline{x}_\theta^* = 0$ to obtain

$$- \underline{x}_\psi \cdot \underline{F} + \kappa_\psi = 0 \tag{22a}$$

and

$$- \underline{x}_\theta \cdot \underline{F} + \kappa_\theta = 0 \ , \tag{22b}$$

where $\underline{F} \equiv \partial^2 L/\partial t \partial \underline{x}_t + B(\partial/\partial\theta)B^{-1}\partial L/\partial \underline{x}_\theta + B(\partial/\partial z)B^{-1}\partial L/\partial \underline{x}_z$. Differentiation of Eqs. (22a) and (22b) with respect to $\theta$ and $\psi$, and algebraic elimination of $\kappa_{\theta\psi} = \kappa_{\psi\theta}$ yield

$$\underline{x}_\psi \cdot \underline{F}_\theta - \underline{x}_\theta \cdot \underline{F}_\psi = 0 \ . \tag{23}$$

Equation (23) is the nonlinear equation of motion for transverse incompressible displacements.

Consider time-dependent displacements of infinitesimal amplitude with respect to a time-independent equilibrium. The linearized equation of motion is

$$\delta\underline{x}_\psi \cdot \underline{F}_\theta + \underline{x}_\psi \cdot \delta\underline{F}_\theta - \delta\underline{x}_\theta \cdot \underline{F}_\psi - \underline{x}_\theta \cdot \underline{\delta F}_\psi = 0 \ . \tag{24}$$

The linearized incompressibility condition becomes

$$\delta \underline{x}_{\psi} \cdot \underline{x}_{\theta}^{*} + \underline{x}_{\psi} \cdot \delta \underline{x}_{\theta}^{*} = \delta x_{\psi}\, y_{\theta} + x_{\psi}\, \delta y_{\theta} - \delta x_{\theta} y_{\psi} - x_{\theta}\, \delta y_{\psi} = 0 \ . \tag{25}$$

In Eqs. (24) and (25), $\delta$ is a linear operator that generates linear displacements of $\underline{x}$ and commutes with partial derivatives with respect to $\psi$, $\theta$, z, and t. We employ the contravariant representation of the linearized displacement $\underline{\xi} \equiv \delta \underline{x}$ used in Ref. 14,

$$\underline{\xi} = X \underline{x}_{\psi} + Y \underline{x}_{\theta} \tag{26}$$

where

$$X = \underline{\xi} \cdot \nabla \psi, \ Y = \underline{\xi} \cdot \nabla \theta \quad .$$

The linearized incompressibility condition Eq. (25) becomes[14]

$$B(X/B)_{\psi} + Y_{\theta} = 0 \ . \tag{27}$$

At this point, assume a complex-exponential normal mode: $X = X_m(\psi)\exp(im\theta - i\omega t)$ + c.c., with $m > 0$. The subscript m will ordinarily be omitted, except where needed for clarity. Use of Eqs. (24-27) and the definition of $\underline{F}$ yields after an abundance of algebra

$$\frac{\partial}{\partial\psi}\left[\rho T r^2 B \frac{\partial}{\partial\psi}\left(\frac{X}{B}\right)\right] - \frac{m^2 \rho T}{r^2 B^2} X + (\rho\omega^2 - \rho T)_\psi \frac{X}{B} - \frac{2m^2 k \bar{p}_\psi}{rB} X$$

$$- m^2 B \frac{\partial}{\partial z}\left(\frac{Q}{r^2 B^3}\frac{\partial}{\partial z} X\right) + \frac{\partial}{\partial\psi}\left\{B \frac{\partial}{\partial z}\left[\frac{Qr^2}{B}\frac{\partial}{\partial z}\left(B \frac{\partial}{\partial\psi}\frac{X}{B}\right)\right]\right\} = 0 \quad , \qquad (28)$$

where $\rho T \equiv \rho[\omega^2 - m\omega(\Omega_1 + \Omega_2) + m^2\Omega_1\Omega_2] = \rho\omega^2 - m\omega\mathscr{X} - m^2\mathscr{Y}$ , $(\partial/\partial t) = - i\omega$, $k = r_{zz}$ is the normal curvature, and $\bar{p} \equiv (p_\perp + p_\parallel)/2$. X satisfies the boundary conditions $X = 0$ at the lateral boundary and either $X = 0$ (end shorted) or $\partial X/\partial z = 0$ (insulated) at the axial end plate.[14] Another boundary condition needed at the ends is $B_\psi = 0$ as a consequence of $p_\perp = p_\parallel = 0$.

Equation (28) can be rewritten in terms of the normal displacement $\xi \equiv \underline{\xi}\cdot\nabla\psi/|\nabla\psi| = X/rB$ and the complex-valued Fourier coefficient $\xi_m$ ,

$$\frac{\partial}{\partial\psi}\left(\rho T r^4 B \frac{\partial}{\partial\psi}\xi\right) + (1 - m^2)\rho\frac{T}{B}\xi + r^2\rho_\psi\omega^2 \xi - m^2 kr\, 2\bar{\rho}_\psi \xi$$

$$- m^2 rB \frac{\partial}{\partial z}\left[\frac{Q}{r^2B^3}\frac{\partial}{\partial z}(rB\xi)\right] + r\frac{\partial}{\partial\psi}\left\{B \frac{\partial}{\partial z}\left[\frac{Qr^2}{B}\frac{\partial}{\partial z}\left(B\frac{\partial}{\partial\psi} r\xi\right)\right]\right\} = 0 \ . \qquad (29)$$

We find that both forms of the linearized equation of motion for the perturbed field-line displacement are useful in the applications addressed in the remaining sections of this paper.

For use later on, we also give a line-averaged version of Eq. (28):

$$\langle \rho r^2 BT(X/B)_\psi \rangle_\psi - m^2 \langle \rho TX/r^2 B^2 \rangle$$

$$+ \langle (\rho\omega^2 - \rho T)_\psi X/B \rangle - 2m^2 \langle k\bar{p}_\psi X/rB \rangle$$

$$- \langle Qr^2 (B_\psi/B)_z (B(X/B)_\psi)_z \rangle = 0 \ , \qquad (30)$$

where $\langle \bullet \rangle \equiv \int (\bullet)\, dz/B$. (This version is useful in the treatment of flute-like modes, for which X is either exactly or approximately independent of z.) Use has been made here of the open-ended boundary conditions $X_z = 0$ and $B_\psi = 0$. (If the conducting boundary conditions are used, then flute-like modes are excluded.)

With Eqs. (28) and (29) we can derive a local stability condition for three-dimensional systems directly. This extends the two-dimensional local stability criterion presented in Sec. X of Ref. 13. Consider the eikonal limit of Eqs. (28) and (29) in which both $|(\partial/\partial z) \approx ik| \to \infty$ and $m \to \infty$. The resulting characteristic equation is

$$\rho\omega^2 - m\omega\mathscr{X} - m^2\mathscr{Y} - k^2 Q = 0 \ , \tag{31a}$$

which yields the following sufficient conditions for local stability at finite beta:

$$Q > 0, \ \mathscr{X}^2 + 4\rho\mathscr{Y} > 0 \ . \tag{31b}$$

The first inequality is the firehose stability condition (9). A system that satisfies (31b) is stable to breaking up into modes of arbitrarily short wavelength both parallel and perpendicular to the magnetic field. We shall restrict ourselves to systems that satisfy Eq. (31b) in the rest of our analysis.

## C. Energy Theorem

The system considered here is non-dissipative and possesses a conserved energy that is directly calculable from the Lagrangian. Assume a variation in the displacement caused by an infinitesimal time translation, $\delta\underline{x} = \Delta t\ \partial\underline{x}/\partial t$, then

$$\delta I = \delta\int_{t_1}^{t_2} dt\int dvol\ [L - \kappa(B\ \underline{x}_\psi \cdot \underline{x}_\theta^* - 1)] = \Delta t\int dvol\ [L(t_2) - L(t_1)]$$

$$= \Delta t\int_{t_1}^{t_2} dt\int d\theta d\psi dz\ \frac{\partial\underline{x}}{\partial t}\cdot(-B^{-1}\ \underline{F} + \kappa_\theta\underline{x}_\psi^* - \kappa_\psi x_\theta^*) + \Delta t\int dvol\ \frac{\partial\underline{x}}{\partial t}\cdot\frac{\partial L}{\partial\underline{x}_t}\Bigg|_{t_1}^{t_2} .$$

Equations (19) and (21) have been used to obtain this. It follows that

$$\int dvol\left[\left(\frac{\partial\underline{x}}{\partial t}\cdot\frac{\partial L}{\partial\underline{x}_t} - L\right)_{t_2} - \left(\frac{\partial\underline{x}}{\partial t}\cdot\frac{\partial L}{\partial\underline{x}_t} - L\right)_{t_1}\right] = 0 \quad ;$$

and hence,

$$\mathscr{H} = \int\frac{d\psi d\theta dz}{B}\ \frac{\partial\underline{x}}{\partial t}\cdot\frac{\partial L}{\partial\underline{x}_t} - L$$

$$= \int\frac{d\psi d\theta dz}{2B}\ (\rho|\underline{x}_t|^2 + \mathscr{Y}|\underline{x}_\theta|^2 + Q|\underline{x}_z|^2) = \text{const.} \qquad (32)$$

This constraint of the nonlinear motion is the system energy; the first term in the parenthesis is the kinetic energy and the second and third terms are the potential energies associated with angular momentum density (an FLR effect) and field-line tension.

There is also a conserved energy for a system that is linearly perturbed from a stationary equilibrium. We expand the energy $\mathscr{H}$ in a Taylor series each of whose terms is conserved,

$$\mathscr{H} = \mathscr{H}^{(o)} + \Delta\mathscr{H} + \frac{\Delta^2}{2}\mathscr{H} + \ldots \quad , \tag{33}$$

where $\mathscr{H}^{(o)} = \int d\mathrm{vol}\,(\mathscr{Y}|\underline{x}_\theta^{(o)}|^2 + Q\,|\underline{x}_z^{(o)}|^2)/2$ in the "null representation" defined in Ref. 13, i.e., $\underline{x}_t^{(o)} \equiv 0$, and $\Delta$ is the linear displacement operator, e.g., $\Delta f(\underline{x}) = \Delta\underline{x}\cdot\partial f/\partial\underline{x} \equiv \underline{\xi}\cdot\partial f/\partial\underline{x}$. The equilibrium is determined by $\Delta\mathscr{H} = 0$ subject to the Jacobian constraint, because it is stationary. Solutions of the equilibrium problem satisfy Eqs. (22a) and (22b) with $\underline{x}_t = 0$. Integration by parts, use of the equations of motion and the incompressibility constraint, and a few pages of algebra reduce the second-order contribution to Eqs. (32) and (33) to a bilinear conserved energy,

$$\begin{aligned}\mathscr{H}^{(2)} &= \frac{\Delta^2}{2}\int \frac{d\psi d\theta dz}{B}\,[\rho|\underline{x}_t|^2 + \mathscr{Y}|\underline{x}_\theta|^2 + Q|\underline{x}_z|^2 - \kappa(B\underline{x}_\psi \cdot \underline{x}_\theta^* - 1)]\\ &= \int \frac{d\psi d\theta dz}{2B}\left\{\rho\left(\frac{X_t^2}{r^2B^2} + r^2\,Y_t^2\right) - 2\bar{p}_\psi\, rBk\,\frac{X^2}{r^2B^2}\right.\\ &\quad \left. + Q\left(\frac{X_z^2}{r^2B^2} + r^2\,Y_z^2\right) + \mathscr{Y}\left[\frac{X_\theta}{r^2B^2} - \frac{X^2}{r^2B^2} + \left(\frac{X}{rB} - rB\,\frac{\partial}{\partial\psi}\,\frac{X}{B}\right)^2\right]\right\}.\end{aligned} \tag{34}$$

The first term in Eq. (34) is the kinetic energy; the second term is the quasi-gravitational potential energy associated with guiding-center-drift motion in a curved magnetic field; the third term is the potential energy due to bending the magnetic field lines; and the fourth and last term is the quasi-elastic potential energy associated with FLR. The energy integral for a paraxial system not restricted to axisymmetry was derived omitting FLR effects in Sec. V of Ref. 14. The FLR potential energy for a system with no axial variation was calculated by Newcomb in Ref. 13. Equation (34) consolidates these earlier results for an axisymmetric equilibrium. We refer the interested reader to Refs. 13 and 14 for algebraic details on the derivation of $\mathscr{H}^{(2)}$.

The conserved energy gives valuable insight into the low-frequency stability of the plasma. If the plasma is unstable, the kinetic energy term, which is always nonnegative, grows at the expense of the potential energy terms. The sum of the potential energy terms must then be negative and growing in magnitude. For $Q \geq 0$, the line-bending term is always positive and stabilizing. The second and fourth terms can be of either sign and, hence, can potentially drive instability. The familiar pressure-weighted curvature term is destabilizing when $\bar{p}_\psi k > 0$. The FLR term is destabilizing when $\mathscr{Y} < 0$, because the square bracket multiplying $\mathscr{Y}$ is nonnegative. We note in the definition of $\mathscr{Y}$ that when the $\underline{E}\mathrm{x}\underline{B}$ rotation exceeds the diamagnetic-like and $\nabla$B-like drift frequencies $\mathscr{Y}$ is always negative.

A sufficient condition for stability is that the potential energy $U^{(2)}$ be positive for all perturbations $\xi$, i.e.,

$$U^{(2)} \geq 0 \ , \tag{35}$$

where

$$U^{(2)} = \int \frac{d\psi d\theta dz}{2B} \left\{ -2\bar{p}_{\psi}\, rBk\, \frac{X^2}{r^2B^2} + Q\left(\frac{X_z^2}{r^2B^2} + r^2\, Y_z^2\right) \right.$$

$$\left. + \mathcal{Y}\left[\frac{X_\theta^2}{r^2B^2} - \frac{X^2}{r^2B^2} + \left(\frac{X}{rB} - rB\,\frac{\partial}{\partial\psi}\,\frac{X}{B}\right)^2\right]\right\} \quad . \tag{36}$$

For a low-beta flute mode, perturbations with $X_z = Y_z = 0$ minimize the strongly stabilizing line-bending energy. For $\mathcal{Y} \geq 0$, we note that

$$U^{(2)} \geq \int \frac{d\psi d\theta dz}{2B}\left[-\, 2\bar{p}_{\psi}\, rBk\, \frac{X^2}{r^2B^2} + \mathcal{Y}\left(\frac{X_\theta^2}{r^2B^2} - \frac{X^2}{r^2B^2}\right)\right] \quad . \tag{37}$$

A sufficient condition for finite-m flute stability when $\mathcal{Y} \geq 0$ is that the right side of Eq. (37) be nonnegative on every field line, viz.

$$\int \frac{dz}{r^2B^3}\,[-\, 2\bar{p}_{\psi}\, rBk + (m^2 - 1)\mathcal{Y}] \geq 0 \quad . \tag{38}$$

Equation (37) demonstrates that with $\mathcal{Y} > 0$, $m = 1$ flute modes are least stabilized by FLR and stabilization increases with $(m^2-1)\mathcal{Y}$. In its most general form, Eq. (34), the energy theorem can provide both useful insight into the interplay of stabilizing and destabilizing physical mechanisms and a valuable diagnostic check on our numerical solution of Eq. (28). An improved energy theorem that recovers stabilizing gyroscopic effects can be obtained by transforming to a rotating frame as in Sec. XV of Ref. 13.

## III. NUMERICAL SOLUTION OF THE STABILITY EQUATION

One of the principal objectives of this work has been the development of the FLORA computer code to numerically solve the linear stability equation, Eq. (29), as an initial-value problem. The solution allows us to prescribe a wide variety of two-dimensional equilibrium configurations without restriction to the specialized profiles that admit analytical solution. It also facilitates more realistic stability analyses of experimental situations and reactor designs. Analytical solutions of the stability equation will be presented in subsequent sections.

FLORA first computes a paraxial equilibrium with finite pressure and then integrates the linearized stability equation. The vacuum magnetic field is a function of z and the parallel plasma pressure as functions of B and $\psi$ must be provided. Condition (3) (parallel pressure balance) then determines $p_\perp$ by analytical differentiation of $p_\parallel/B$ with respect to B, whereupon condition (2) (perpendicular pressure balance) gives an algebraic relation for $B(\psi,z)$:

$$B^2 + 2p_\perp(B,\psi) = B^2_{vac}(z) \ . \tag{39}$$

The radius of the lines of force $r(\psi,z)$ is numerically calculated from

$$r^2 = 2\int_0^\psi d\psi'/B(\psi',z) \ , \tag{40}$$

and the curvature $k = r_{zz}$ is determined by analytical differentiation under the integral. The mass density $\rho$ and the FLR coefficients $\mathscr{X}$ and $\mathscr{Y}$, as functions of $\psi$ and B, must also be provided as input to the calculation.

With all the necessary coefficients determined, the stability equation is integrated by means of standard finite-difference techniques. Reintroducing time derivatives in Eq. (29), one obtains

$$- \frac{\partial}{\partial\psi} \left[ \left( \rho \frac{\partial^2}{\partial t^2} + im\mathscr{X}\frac{\partial}{\partial t} + m^2\mathscr{Y} \right) r^4 B \frac{\partial}{\partial\psi} \xi \right] - \frac{(1 - m^2)}{B} \left( \rho \frac{\partial^2}{\partial t^2} + im\mathscr{X}\frac{\partial}{\partial t} + m^2\mathscr{Y} \right) \xi$$

$$- r^2 \rho_\psi \frac{\partial^2 \xi}{\partial t^2} - 2m^2 rk\bar{p}_\psi \xi - m^2 rB \frac{\partial}{\partial z} \left[ \frac{Q}{r^2 B^3} \frac{\partial}{\partial z} (rB\xi) \right] + \frac{r\partial}{\partial\psi} \left\{ B \frac{\partial}{\partial z} \left[ \frac{Qr^2\partial}{B\partial z} \left( B\frac{\partial}{\partial\psi} r\xi \right) \right] \right\} = 0. \tag{41}$$

The flux coordinates z and $\psi$ are analytically transformed to new coordinates u(z) and v($\psi$), and the spatial derivatives in Eq. (41) are represented as second-order-accurate centered finite differences with respect to u and v. This facilitates the use of a nonuniform z, $\psi$ mesh to improve spatial resolution where desirable, while preserving second-order accuracy. The highest spatial derivatives appearing in Eq. (41) are represented by 9-point operators.

To understand the finite-differencing of the time derivatives, consider Eq. (40) written in the symbolic form

$$\mathscr{A} \frac{\partial^2}{\partial t^2} \xi + i \mathscr{B} \frac{\partial}{\partial t} \xi + \mathscr{C} \xi = 0 \ , \tag{42}$$

where $\mathscr{A}$, $\mathscr{B}$, and $\mathscr{C}$ are linear operators with real coefficients. We have recast Eq. (42) in the partially implicit form

$$\frac{\mathscr{A}}{\Delta t^2} (\xi^{n+1} - 2\xi^n + \xi^{n-1}) + i \frac{\mathscr{B}}{2\Delta t} (\xi^* - \xi^{n-1})$$

$$+ \mathscr{C} \left[ \varepsilon\xi^{n+1} + \frac{(1 - \varepsilon)}{4} (\xi^{n+1} + 2\xi^n + \xi^{n-1}) \right] = 0 \ , \tag{43}$$

where the superscripts indicate the time level, $\varepsilon$ is a numerical centering parameter with typical value $0 \leq \varepsilon << 1$, and $\xi^*$ is the previous iterant value of $\xi^{n+1}$. The solutions of Eq. (43) for the real and imaginary parts of $\xi^{n+1}$ are coupled explicitly to the imaginary and real parts of $\xi^{*}$, respectively, and to both the real and imaginary parts of $\xi^{n}$ and $\xi^{n-1}$. The real and imaginary parts of $\xi^{n+1}$ are not directly coupled to one another within an iteration, which reduces the size of the matrix of coefficients by one-half but requires an iterative solution for the real and imaginary parts of $\xi^{n+1}$. The solution to the banded-matrix equation that results from Eq. (43) is obtained by a machine-language-coded direct solver in which a lower-upper (LU) decomposition is performed only once at $t = 0$ and a back-substitution is done on each iteration. A sufficient condition on the convergence of the iteration is given locally in $\psi$ and $z$ by

$$|m\mathscr{X}\Delta t/2\rho| < 1$$

for equilibria that vary weakly in space. This is equivalent to the condition that the real part of the linear mode frequency be accurately resolved when $\mathscr{X}/\rho$ is finite (see Sec. IV).

The implicit time-differencing of the $\mathscr{C}\xi$ term in Eqs. (42) and (43) dispenses with the Alfvén Courant condition $v_A\Delta t/\Delta z < 1$, where $v_A = (B^2/\rho)^{1/2}$. With $\mathscr{X} = \mathscr{Y} = 0$, $(|\partial\xi/\partial\psi|, |\partial\xi/\partial\theta|) << |\partial\xi/\partial z|$, a uniform magnetic field; and a cold uniform plasma, Eq. (41) describes shear Alfvén waves: $(\rho\partial^2/\partial t^2 + B^2\partial^2/\partial z^2)\ \xi = 0$. An explicit time integration of this would require that a Courant condition be satisfied in order to avoid numerical instability. The resulting time step at marginal stability, $\Delta t_c = \Delta z/v_A$, would be much smaller than that necessary to accurately resolve a simple curvature-driven interchange mode, viz. $\gamma\, \Delta t_c = \mathcal{O}(\beta \Delta z^2 / R_p R_c)^{1/2} << 1$, where $\gamma$ is the interchange growth rate, $\beta$ is the ratio of the plasma pressure to the magnetic energy density, $\Delta z$ is the axial grid spacing, $R_p$ is the plasma radius, and $R_c^{-1}$ is the flux-line curvature. The partially implicit time integration indicated in Eq. (43) allows us to use a larger time step appropriate in resolving the characteristic FLR frequencies and the instability growth rate.

Before leaving this section, we comment on an alternative numerical scheme for solving the stability problem. Suppose one establishes an array $\underline{s}\, \exp(-i\omega t)$ + c.c. containing all the values of $\xi(\psi,z,t)$ defined on the two-dimensional mesh. The linear operators $\mathscr{A}$, $\mathscr{B}$, and $\mathscr{C}$ in Eq. (42) are then deduced from the spatial difference operators on $\xi$ used to represent Eq. (41) and can be cast in matrix form. One then Fourier analyzes in time to examine the normal modes, and Eq. (41) becomes

$$(-\,\omega^2 \underline{\underline{\mathscr{A}}} + \omega \underline{\underline{\mathscr{B}}} + \underline{\underline{\mathscr{C}}}) \cdot \underline{s} = 0 \ , \tag{44a}$$

whose nontrivial solution is

$$\det(-\,\omega^2 \underline{\underline{\mathscr{A}}} + \omega \underline{\underline{\mathscr{B}}} + \underline{\underline{\mathscr{C}}}) = 0 \ . \tag{44b}$$

The order of this characteristic polynominal is twice the total number of mesh points, and the solutions for $\omega$ are finite-difference approximations to the true eigenfrequencies.

A characteristic polynominal equation similar to Eq. (44b) is generated by using a Galerkin method in which a set of orthogonal basis functions (finite elements) with analytical spatial derivatives are employed to represent $\xi(\psi,z)$. This approach has been used in Ref. 28 to analyze the low-frequency stability of a low-beta quadrupole tandem mirror including $\underline{E}x\underline{B}$ rotation and FLR effects. With this method it may be necessary to solve for all of the roots of the characteristic polynominal to ensure that the least stable (or most unstable) root is found. In contrast, the most unstable mode always dominates the linear impulse response in the integration of the initial-value problem after a few e-foldings. Of course, the e-folding times become longer and longer as marginal stability is approached, at which point relative inaccuracies in the observed growth rates due to finite differencing are magnified in the integration of the initial-value problem.

## IV. ANALYTICAL AND NUMERICAL RESULTS FOR SPECIAL CASES

In this section we present analytical and numerical solutions of the low-frequency stability equations, Eqs. (28) and (29), in several limiting cases. These calculations illustrate many important characteristics of interchange and rotational stability with FLR and conducting wall effects. The analytical solutions provide valuable insight and serve as a standard for comparison of the corresponding results from FLORA.

## A. Low-Beta Limits

We consider first the so-called "low-beta limit", where $\beta$ is defined as the material-to-magnetic pressure ratio. To state the ordering rules of the $\beta$ expansion as concisely as possible, we put

$$\rho,\ M,\ K,\ p_\perp,\ p_\parallel,\ B_\psi,\ X_z = \mathcal{O}(\beta)\ ,$$

$$m,\ \omega,\ \phi,\ \Omega_1,\ \Omega_2,\ B,\ k,\ X,\ X_\psi = \mathcal{O}(1)\quad . \tag{45}$$

To leading order, B is independent of $\psi$ and X is independent of z. The two characteristic frequencies become

$$\Omega_1 = \phi_\psi,\ \Omega_2 = \phi_\psi + \frac{B}{2\rho} M_\psi\ , \tag{46}$$

wherein K no longer appears. The flute condition, $X_z = 0$, is enforced by the large terms in Eq. (28). These, however, are annihilated by the averaging operation in Eq. (30), from which is derived the final eigenequation. This takes the form of

$$(2\psi\ \Lambda\ X_\psi)_\psi - (m^2/2\psi)\ \Lambda X$$

$$+ m(\omega f_\psi + m g_\psi)\ X + m^2\ H_\psi\ X = 0\ , \tag{47}$$

where

$$\Lambda = e\omega^2 - fm\omega - gm^2 \ , \tag{48a}$$

$$e = \langle \rho/B \rangle \ , \tag{48b}$$

$$f = \langle \mathscr{X}/B \rangle = \langle \rho(\Omega_1 + \Omega_2)/B \rangle \ , \tag{48c}$$

$$g = \langle \mathscr{Y}/B \rangle = - \langle \rho\Omega_1 \, \Omega_2/B \rangle \ , \tag{48d}$$

$$H = - \langle 2k\bar{p}/rB \rangle \ . \tag{48e}$$

We see, then, that the z-dependence in this simple case can be integrated out completely.

Assume first $\Omega_1 = \Omega_2 = 0$ (no rotation, no FLR), or equivalently, $f = g = 0$. Equation (47) then simplifies to

$$\omega^2 \left[ -(2\psi e \, X_\psi)_\psi + \frac{m^2 e}{2\psi} \, X \right] = m^2 \, H_\psi \, X \ , \tag{49}$$

or finally, if we multiply by X and integrate,

$$\omega^2 \int e \left( \frac{m^2 X^2}{2\psi} + 2\psi \, X_\psi^2 \right) d\psi = m^2 \int H_\psi \, X^2 \, d\psi \ . \tag{50}$$

This implies instability, $\omega^2 < 0$ (at least in the case of large m), unless H is everywhere an increasing function of $\psi$. Assuming $H \to 0$ at the lateral boundary, we see that $H < 0$ is necessary for stability against the flute mode.

Let us observe now that k/r in the present case is a function only of z. To leading order in $\beta$, B is a function only of z, whereupon, by differentiation of $r^2 B = 2\psi$ = const., we readily obtain

$$k/r = r_{zz}/r = -\frac{1}{2} B^{1/2} (B^{-3/2} B_z)_z \ . \tag{51}$$

Using also the boundary condition $\bar{p} = 0$ at the ends, we have finally

$$H = \left[ \bar{p} B^{-1/2} (B^{-3/2} B_z)_z \right]$$

$$= - \langle B^{-1/2} B_z \ (\bar{p} B^{-3/2})_z \rangle \ . \tag{52}$$

If the monotonicity condition (12) is satisfied, then $\bar{p}B^{-3/2}$ is always a decreasing function of B, and H according to Eq. (52) is positive, implying instability.[14] If it is not satisfied (as in the case of a sloshing-ion distribution), then H can be of either sign.

## B. Eikonal Approximation

For large m, the so-called "eikonal approximation" is applicable, whereby Eq. (49) is simplified to

$$m^2 \ X \ (H_\psi - \omega^2 e/2\psi) = 0 \ . \tag{53}$$

Let us assume $H_\psi < 0$ (the usual case). We then obtain the standard result for the local growth rate $\bar{\gamma}$ on each individual flux surface in the limit of no rotation, no FLR, and large m:

$$\bar{\gamma}^2 = -\omega^2 = -2\psi H_\psi/e \ . \tag{54}$$

We see that the growth rate approaches a finite limit as $m \to \infty$.

For nonzero $\Omega_1$, $\Omega_2$, the corresponding approximation yields a different result, i.e., $\Lambda = 0$, or

$$e\omega^2 - fm\omega - gm^2 = 0 \ , \tag{55}$$

as the local dispersion relation. In this case, then, the angular frequency $\omega$ (or in the unstable case, the growth rate) is a linearly increasing function of m.

To the order of approximation represented by Eq. (55), the criterion of stability is simply $\mathcal{Q} > 0$, where

$$\mathcal{Q} = \frac{1}{4} f^2 + eg \ . \tag{56}$$

Again it is found that the gyroscopic term (coefficient f) is always stabilizing, whereas the quasielastic term (coefficient g) is stabilizing only if positive. The combined effect of both terms (properly weighted) is measured by the quantity $\mathcal{Q}$. Note that in an axially uniform system, the stability condition (56) is identical to the local stability condition (31b). However, $\mathcal{Q}$ could be negative in an axially non-uniform system that is locally stable everywhere.

Using formulas (15) and (48) for e, f, and g in terms of fundamental quantities, we rewrite (56) as

$$\mathscr{Q} = \langle\rho\Omega/B\rangle^2 - \langle\rho/B\rangle\,\langle\rho\Omega^2/B\rangle + \frac{1}{16}\,\langle\rho/B\rangle\,\langle BM_\psi{}^2/\rho\rangle \quad , \tag{57}$$

where $\Omega = \frac{1}{2}(\Omega_1 + \Omega_2)$. This quantity $\Omega$, the arithmetic mean of the two characteristic frequencies, is the so-called "canonical" angular velocity of Ref. 13. In the following, we use the terms "radial" and "axial shear" to refer specifically to the dependence of $\Omega$ (rather than $\Omega_2$, say) on $\psi$ and z.

The two terms in Eq. (57) involving $\Omega$ represent the effect of axial shear, which is always destabilizing. Indeed, these terms cancel exactly in the case of zero shear ($\Omega_z$ vanishing identically), whereas in every other case the negative term is the larger of the two (Cauchy-Schwartz inequality). On the other hand, the FLR term (the term involving M) is always positive, hence stabilizing. We see that the shear-driven instability can always be suppressed by an FLR term of sufficiently large magnitude.

To illustrate also the stabilization effect of FLR on the curvature-driven mode, let us consider next the case of weak rotation and weak FLR: $\Omega_1$ and $\Omega_2$ both small (say of order $\varepsilon$) compared with $\bar{\gamma}$ or $\omega$. In this case too, the eikonal approximation is applicable (for m of order $\varepsilon^{-1}$), and the local dispersion relation to which it leads is

$$\Lambda + e\bar{\gamma}^2 = e(\omega^2 + \bar{\gamma}^2) - fm\omega - gm^2 = 0 \quad . \tag{58}$$

We are again using $\bar{\gamma}$ to denote the classical growth rate, as given by formula (54). The criterion of stability is

$$m^2\mathscr{Q} \;>\; e\bar{\gamma}^2 \; . \tag{59}$$

Thus, if the positive-$\mathcal{D}$ condition is satisfied, there exists a critical value of m, $m_o = \bar{\gamma}(e/\mathcal{D})^{1/2}$, such that the curvature-driven mode is stabilized for all $m > m_o$.

Plasma rotation is an important source of free energy that can drive MHD instability. This is illustrated in the rotational instability of the rigid-rotor equilibrium of Ref. 17, which is discussed in Sec. IV.C. Axial or radial variation in the plasma rotation can also lead to instability. Consider plasmas with significant $\underline{E}\times\underline{B}$ rotation and weak FLR such that $\mathcal{X} = 2\rho\phi_\psi$ and $\mathcal{Y} = -\rho\phi_\psi^2$. In this limit the high-m, low-beta dispersion relation for flute modes, Eq. (55), gives

$$\omega = \frac{mf}{2e} \pm \frac{m}{e}\,\mathcal{D}^{1/2} \quad , \tag{60}$$

where with no FLR $\Omega = \Omega_E$ and

$$f \rightarrow \langle 2\rho\Omega/B\rangle \tag{61a}$$

$$g \rightarrow -\langle \rho\Omega^2/B\rangle \tag{61b}$$

$$\mathcal{D} \rightarrow \langle \rho\Omega/B\rangle^2 - \langle \rho/B\rangle\,\langle \rho\Omega^2/B\rangle \quad . \tag{61c}$$

$\mathcal{D}$ is always nonpositive by the Cauchy-Schwartz inequality. If $\Omega$ is axially uniform, the eikonal limit of Eq. (47) gives

$$\frac{m^2}{2\psi}\,\Lambda X + m(\omega f_\psi + m g_\psi)\,X + m^2 H_\psi X = 0 \tag{62}$$

with $\Lambda = \mathcal{O}(1)$. The resulting eigenfrequency is

$$\omega = m\Omega \pm i \left(-2\psi \frac{\langle B^{-1}\partial\rho/\partial\psi\rangle}{\langle\rho/B\rangle} \Omega^2 + \bar{\gamma}^2\right)^{1/2} \tag{63}$$

where $\bar{\gamma}^2$ is given in Eq. (54). The first term in the parentheses is a Rayleigh-Taylor centrifugal drive term.

The existence of instablity driven by $\underline{E}\times\underline{B}$ rotation could be anticipated from our energy theorem (34 - 36) for systems with $\mathscr{Y} < 0$. Equation (63) suggests the possibility that the combination of rotation and a hollow density profile, $\langle B^{-1}\partial\rho/\partial\psi\rangle > 0$, might stabilize a configuration with bad curvature.[35] This has been quantitatively studied with FLORA and will be reported elsewhere.[36]

Figures 1 to 3 exhibit a numerical study with FLORA of modes excited by sheared rotation. In this case $\Omega$ was equal to a constant value in the central cell and to a different constant value in the anchor cell of a simple tandem mirror. The tandem equilibrium considered (Fig. 1) was interchange unstable because of axially sheared rotation and bad curvature (Fig. 2). The growth rates are shown to increase with increasing shear and mode number m (Fig. 3). The eikonal theory does very well in predicting growth rates for the entire range of m and the shear values indicated. The analytical growth rates for finite shear are given by Eq. (55) and for no shear by Eq. (63). In the presence of trapped particles, the low-frequency instability excited by axial shear is modified as shown in Ref. 37.

Returning now to the simple case f = g = o (or $\Omega_1 = \Omega_2 = 0$: no rotation, no FLR), we seek a better estimate of the maximum growth rate. This is provided by a simple WKBJ calculation.

The fastest growing interchange eigenmode is localized in $\psi$ around the flux surface on which $\bar{\gamma}$ is a maximum. Introduce the variable u defined by $du = d\psi/2e\psi$ in Eq. (47) with f=g=o, which becomes

$$\frac{\partial^2}{\partial u^2} X + k(u)^2 X = 0 \ , \qquad (64a)$$

where

$$k(u)^2 = -m^2 e^2 (1 + \bar{\gamma}^2/\omega^2) \ . \qquad (64b)$$

Expand $k(u)^2$ in a Taylor series around its maximum at $u_o$ (assumed to occur at an interior point; see Fig. 4a) to deduce the eigenfrequency $\omega$ from the WKBJ condition,

$$\int_{u_2}^{u_2} du \ k(u) \approx \int_{u_1}^{u_2} du \left[ k_o^2 - K \ (u_o - u)^2/2 \right]^{1/2} = (n + 1/2) \ \pi \ , \qquad (65)$$

where $k_o^2 = k(u_o)^2$, $K \equiv -\partial^2(k^2)/\partial u^2$ at $u_o$, and $k_o^2 - K(u_o - u)^2/2 = 0$ at $u = u_1, u_2$. For $m >> 1$, the fastest growing mode has an eigenfrequency

$$\omega^2 = - \gamma_o^2 (1 - |2\psi_o^2 \gamma^2_{\psi\psi}|^{1/2}/m\gamma_o) \ . \qquad (66)$$

This is the lowest radial mode n=o and has no internal nodes. We have defined $\gamma^2_{\psi\psi} \equiv \partial^2 \bar{\gamma}^2/\partial\psi^2$ at $\psi_o(u_o) = Br_o^2/2$ and $\gamma_o^2 \equiv \bar{\gamma}^2$ at $u_o$. The values of $u_o$ and $\gamma_o^2$ in Eq. (66) determined by $dk^2/du = 0$ can be replaced by the values of u and $\bar{\gamma}^2$ where $d\bar{\gamma}^2/du = 0$ (its maximum). The resulting change in Eq. (66) is higher order than $\mathcal{O}(1/m)$. Equation (66) indicates that there is a reduction in growth rate for finite values of m. There would also be a reduction in the growth rate if the mode could not maintain its axial flute character because of line tying at an axial boundary, $X(z = L) = 0$, for example. The stabilization afforded by line bending is illustrated both by the finite positive-definite Q term in Eq. (34) and by the term $k_z^2 \, v_A^2$ in the linear dispersion relation in the next sub-section.

The eigenfunction is centered at $\psi_o$ and has an effective width $\Delta\psi \propto m^{-1/2}$ determined by the turning points, $k(u)^2 \propto \bar{\gamma}(u)^2 + \omega^2 = 0$, and given approximately by

$$\Delta\psi \approx \left| \frac{\omega^2 + \gamma_o^2}{\gamma^2_{\psi\psi}} \right|^{1/2} = \left( \frac{2\psi_o \gamma_o}{m|\gamma^2_{\psi\psi}|^{1/2}} \right)^{1/2} \quad . \tag{67}$$

As expected, the agreement of the numerical results obtained from FLORA with the WKBJ results Eq. (66) for high-m curvature-driven modes at low beta steadily improves as m increases (see plot of eigenfrequencies in Fig. 4b).

## C. Rigidly Rotating θ Pinch

The next example illustrates rotational instability with FLR effects in a straight θ-pinch configuration. Here we recover the stability equation derived earlier in Ref. 17 and obtain good numerical agreement between the numerical results presented there and those obtained by use of FLORA. This earlier research addressed the low-frequency stability of an axially uniform, rigidly rotating θ-pinch with finite β and FLR, with isotropic Maxwellian velocity distribution functions, and with both $\Omega^*$ and $\Omega_E$ constant. With no curvature drive, plasma rotation provides a centrifugal force that can cause instability.

Consider Eq. (28) for a system with a z-independent equilibrium. Fourier analyzing the z dependence of $\xi$, we put $\partial\xi/\partial z = ik\xi$; and we also make the coordinate transformation $\partial/\partial\psi = (rB)^{-1}\,\partial/\partial r$. After a straightforward algebraic manipulation we recover Eq. (10) of Ref. 17

$$\frac{\partial}{\partial r}\left[r^3(\rho T-F^2)\frac{\partial}{\partial r}\xi\right] + r\xi\left[(1-m^2)(\rho T-F^2) + \frac{r\partial}{\partial r}(\rho\omega^2 - F^2)\right] = 0 \;, \qquad (68)$$

where $\mathcal{F}^2 = k^2Q = k^2B^2$ and $\rho T = \rho(\omega - m\Omega_E - m\Omega_{\nabla B})(\omega - m\Omega_E - m\,\Omega^*)$. We note the appearance in the $\mathcal{F}^2$ term of the linear line-bending restoring force so that all modes are stable for sufficiently large $|k|$.

In the absence of FLR, $X = Y = 0$ and $T = \omega^2 = k^2B^2/\rho$, so that Eq. (68) reduces to the well-known dispersion relation for a simple shear Alfvén wave. This provides an elementary check on FLORA: it was found that stable shear Alfvén waves are correctly reproduced within the accuracy limits imposed by the differencing scheme. In Figs. 5 and 6, we compare the eigenfrequencies and radial eigenmodes obtained in Ref. 17 with those obtained with FLORA for the same equilibrium using a 40 x 40 grid and $|\omega^*\Delta t| = 0.02$ for modes with n=0 and m=1 or 2. Frequencies and growth rates are normalized to $\Omega^*$ and are plotted as functions of the normalized shear-Alfvén-wave frequency $kv_A/\Omega^*$, where $v_A^2 = B_o^2/\rho$. The relative plasma pressure on axis is parametrized by $\beta_o \equiv 2p_\perp(0)/B_o^2$ and the plasma rotation speed by $\alpha = 1 + \Omega_E/\Omega^*$. All modes are eventually stabilized at large values of $kV_A$. The agreement of the eigenfrequencies and eigenmodes in FLORA with those in Ref. 17 is good, in keeping with the finite differencing errors. The agreement is better for the eigenfrequencies than it is for the eigenmodes.

## D. Square Plasma Profiles with Wall Effects

A simple, though artificial, model problem that demonstrates the stabilizing effects of both FLR and a nearby conducting wall is given by a system with square radial profiles for the density, pressure components, and FLR coefficients. Consider a low-beta system with two regions in the radial direction and insulated free boundaries axially. The inner (I) and outer (II) regions meet at $\psi_p \equiv Br_p^2/2$. Note that B and hence $r_p$ and $r_w$ are possibly functions of z. The relevant flute-averaged eigenequation for the displacement is given by Eq. (47). With $\rho$, $p_\perp$, $p_{||}$, $\phi_\psi$, and $M_\psi$ constant in the two regions, Eq. (47) simplifies to

$$\frac{\partial}{\partial\psi}\left(\Lambda\psi\frac{\partial}{\partial\psi}X\right) - \frac{m^2\Lambda}{4\psi}X = 0 \quad ; \tag{69}$$

and the derivative $\partial X/\partial\psi$ is discontinuous at $\psi_p$.

With boundary conditions X = 0 at $\psi_w$, regularity at $\psi = 0$, and continuity at $\psi = \psi_p$ the solution of Eq. (69) is

$$X = \begin{cases} \psi^{m/2} , & \psi < \psi_p \\ a\,\psi^{m/2} + b\psi^{-m/2} , & \psi > \psi_p \end{cases} \tag{70}$$

where $a = -(\psi_w^m/\psi_p^m - 1)^{-1}$, and $b = -a\,\psi_w^m$. The eigenvalue $\omega$ is obtained by integrating Eq. (47) with respect to $\psi$ across $\psi_p$ and using the jump in $\partial X/\partial\psi$ deduced from Eq. (70). We obtain the dispersion relation

$$\mathscr{A}\omega^2 + \mathscr{B}\omega + \mathscr{C} = 0 \tag{71}$$

where

$$\mathscr{A} = (\frac{d + 1}{d - 1}) e_{II} + e_I \tag{72a}$$

$$\mathscr{B} = (m - 1)f\Big|_{I}^{II} - m \frac{2d}{d-1} f_{II} \tag{72b}$$

$$\mathscr{C} = m(m - 1) g\Big|_{I}^{II} - m^2 \frac{2d}{d-1} g_{II} - mH\Big|_{I}^{II} , \tag{72c}$$

e, f, g, and H were defined in Eq. (48), and $d \equiv \psi_w^m/\psi_p^m$.

A number of useful conclusions can be drawn immediately. Consider first the limit of a vacuum separating the inner plasma region from the conducting wall. Then $A \rightarrow \langle\rho/B\rangle_I$, $B \rightarrow (1-m) \langle\rho(\Omega_1 + \Omega_2)/B\rangle_I$ and $C \rightarrow m(m-1) \langle\rho\Omega_1\Omega_2/B\rangle_I - 2m \langle k\bar{p}/B\rangle_I$. Because of the low-beta assumption, the dispersion relation is independent of the wall position as long as the plasma is separated by a vacuum from the wall. For m=1, the FLR modifications vanish, the displacement $\xi = X/rB$ is rigid (constant) within the plasma, and the mode is a simple interchange. For m > 1, the gyroscopic effects coming through $\mathscr{B}$ are always stabilizing; and the quasi-elastic term in $\mathscr{C}$ is also stabilizing if $\langle\rho\Omega_1\Omega_2/B\rangle < 0$. The effect of FLR on the discriminant of Eq. (71) increases as $m^2$ for m >> 1.

A new phenomenon emerges when there is plasma in the outer region and the conducting wall is nearby. With $d \rightarrow 1+$ and $(d-1)^{-1} >> 1$, there is a sharp enhancement of the plasma inertia in $\mathscr{A}$ and of the gyroscopic effect in $\mathscr{B}$, both of which are always stabilizing. There is also a strong enhancement of the quasi-elastic effects in $\mathscr{C}$, which are stabilizing if $\langle\rho\Omega_1\Omega_2/B\rangle_{II} < 0$. Additional stabilization is afforded by a nearby conducting wall when the plasma has finite pressure because of the bending of field lines trapped between the plasma and the conducting wall.[31-34]

Consider the evaluation of Eq. (71) when there is a plasma occupying Region I which is surrounded by a vacuum and then a conducting wall. The eigenfrequency resulting from Eqs. (71) and (72) is

$$\omega = \frac{(m-1)f}{2e} \pm \frac{1}{e} \left[(m-1)^2 \mathscr{Q} + (m-1)\, eg - meH\right]^{1/2} , \tag{73}$$

where all quantities are evaluated in the plasma, region I. With $\underline{E} \times \underline{B}$ rotation and no FLR, then $\Omega = \Omega_E$, $f \rightarrow \langle 2\rho\Omega/B \rangle$, and $g \rightarrow -\langle \rho\Omega^2/B \rangle$. Based on the energy theorem, we anticipate the possibility of instability because $\mathscr{Y} < 0$. The first term under the square root in (73) is the destabilizing shear term analyzed earlier. The next term is a destabilizing Rayleigh-Taylor rotational term for $m > 1$: the rotation produces a centrifugal force equivalent to a gravitational force directed outward. The third term under the square root is the pressure-weighted curvature term and is destabilizing for negative average curvature. The rotational effects disappear for the $m=1$ mode, which is a rigid displacement of the plasma.

For the opposite limit of a vacuum region on axis surrounded by a uniform plasma annulus with density, pressure, rotation, and FLR that are constant in radius, the dispersion relation deduced from Eqs. (71) and (72) is

$$\omega = (m+1) \frac{f}{2e} \pm \frac{1}{e} \left[(m+1)^2 \mathscr{Q} - (m+1)\, eg + meH\right]^{1/2} \tag{74}$$

with all quantities evaluated in the plasma, Region II, and $\psi_w^m \gg \psi_p^m$. With rotation and no FLR, the outward directed centrifugal force is stabilizing because the effective gravity and density gradient are parallel causing the second term under the square root, to be positive. Similarly, negative average curvature is now stabilizing because the plasma is hollow. Because the displacement is not rigid for any value of m, rotational stabilization is effective for all m.

The grossest features of radial shear in the $\underline{E}\mathrm{x}\underline{B}$ rotation can be qualitatively illustrated in the sharp-boundary model by allowing a pressureless non-rotating plasma with finite density to occupy what had been the vacuum regions in the two model problems immediately preceding. The only change in the dispersion relations Eqs. (73) and (74) is that the plasma inertia appearing in the denominators of both expressions becomes e(I) + e(II) for $\psi_w^m/\psi_p^m >> 1$. Hence, radial shear in $\Omega_E$ is stabilizing or destabilizing depending on whether the $\Omega_E$ profile is hollow (inverted) or decreasing with radius, respectively. Qualitatively similar results have been obtained in an earlier detailed study that considered low-m rotational stability of a low-beta, infinitely long cylindrical plasma with Gaussian density profile and no magnetic curvature effects.[38] From the analytical results of this subsection we see that radial potential profile control, which is important in reducing radial transport in tandem mirrors with quadrupole plugs, can also improve the MHD stability of a tandem mirror.

In the course of our numerical studies confirming the analytical results of this section, a spurious numerical instability was uncovered. When the plasma equilibrium is uniform in both $\psi$ and z so that the stability equation has constant coefficients throughout, the iterative partial differential equations for Re $\xi$ and Im $\xi$ become singular in their highest $\psi$ derivatives if $\rho\omega^2 - m^2\mathcal{Y} = 0$. This leads to a numerical instability if both $\mathcal{Y} < 0$ and Im $\omega = (-m\,\mathcal{Y}/\rho)^{1/2}$ exceeds the growth rates of all physical instabilities present. However, we have found that the conditions leading to this numerical instability are easily avoided in applications to physical systems.

## E. Bessel Solution

In this subsection, we consider a simple limiting case in which the low-beta eigenequation is explicitly solvable in terms of Bessel functions. Let us assume that the distribution function (in general, a function of magnetic moment $\mu$, energy $\varepsilon$, and $\psi$, as well as of the species index s) depends on $\psi$ only through a factor $\exp(-G\psi)$, where G is a constant (the same for all species). We then have

$$(\rho,M,\bar{p}) = (\rho_o,M_o,\bar{p}_o)\exp(-G\psi) \ , \tag{75}$$

where $\rho_o$, $M_o$, and $\bar{p}_o$ are functions only of z.

Recall now that $\phi$ is expressible in general as $\phi_1(\psi) + \phi_2(\psi,z)$, where $\phi_2$ is determined by the charge neutrality condition and $\phi_1$ is essentially arbitrary. (Within the framework of the collisionless equilibrium theory, it is necessary to prescribe the function $\phi_1$, as one of the side conditions needed in order to specify the equilibrium uniquely.[14]) In the present case, the factor $\exp(-G\psi)$ cancels out of the charge-neutrality condition, with the result that $\phi_2$ is independent of $\psi$, and $\phi_\psi$ reduces to $\phi_{1\psi}$, i.e., to a function only of $\psi$. We now make the further assumption (without any inconsistency, since $\phi_1$ is essentially arbitrary) that $\phi_\psi$ is independent of $\psi$ as well as z. We assume, in short, $\phi_\psi(\psi) = \Omega_e$, where $\Omega_e$ = const.

It follows now that

$$(e,f,g) = (e_o,\ f_o,\ g_o)\exp(-G\psi) \tag{76}$$

where $e_o$, $f_o$, and $g_o$ are constants. Explicitly, we obtain

$$e_o = \langle \rho_o/B \rangle \quad , \tag{77a}$$

$$f_o = 2\Omega e_o \quad , \tag{77b}$$

$$g_o = (\frac{\Sigma^2}{16} - \Omega^2)\ e_o \tag{77c}$$

where

$$\Omega = \Omega_e - \frac{\Sigma}{4} \quad , \tag{77d}$$

$$\Sigma = G \langle M_o \rangle / e_o \quad . \tag{77e}$$

We also have $H = H_o \exp(-\ \psi)$, where $H_o$ is given by the same formula Eq. (52) as H itself, except that $p_o$ replaces $p$.

The eigenequation now reduces to

$$(\sigma^2 - \frac{1}{16} m^2 \Sigma^2)\ [(2\psi X_\psi)_\psi - \frac{m^2}{2\psi} X - 2\psi G X_\psi]$$
$$- G(m^2\Omega^2 + 2m\Omega\sigma + \frac{1}{16} m^2 \Sigma^2 + m^2\ T)\ X = 0 \quad , \tag{78}$$

where $T = H_o/e_o$ and

$$\sigma = \omega - m\Omega \quad . \tag{79}$$

The angular frequency designated as $\Omega$ is essentially the "canonical" angular velocity of Ref. 13, and $\sigma$ is simply the mode angular frequency $\omega$ transformed to a rotating reference frame of angular velocity $\Omega$.

Consider now the following limit: $G \to 0$, but with $\Omega^2$ and $H_o$ both going to infinity as $G^{-1}$. The eigenequation now reduces to

$$(2\psi X_\psi)_\psi + (\kappa^2 - \frac{m^2}{2\psi}) X = 0 \quad , \tag{80}$$

where

$$\kappa^2 = - \frac{m^2 G(\Omega^2 + T)}{\sigma^2 - m^2 \Sigma^2/16} \quad . \tag{81}$$

But this is simply Bessel's equation of order m (after a trivial change of variable). The explicit solution (with the boundary condition $X \to 0$ at $\psi = 0$) is $X = J_m(\kappa(2\psi)^{1/2})$.

Let us assume for simplicity a rigid boundary at $\psi = \psi_w$, at which the boundary condition $X = 0$ will obtain. The eigenfrequencies are then given by the formula

$$\sigma^2 = \frac{1}{16} m^2 \Sigma^2 - \frac{2m^2\psi_w}{\gamma_{mn}^2} G(\Omega^2 + T) \quad , \tag{82}$$

where $\gamma_{mn}$ denotes the $n$th zero by $J_m$. The worst case is the lowest radial mode, m=1, n=1, $\gamma_{11} = 3.8317$, resulting in the stability criterion

$$\Sigma^2 > \frac{32\ \psi_w}{\gamma_{11}^2} G(\Omega^2 + T) \quad . \tag{83}$$

The term on the left represents the stabilizing FLR effect (proportional to $<M_o>^2$, or $\Sigma^2$), and the destabilizing terms on the right are, respectively, the result of centrifual drive ($\sim\Omega^2$) and of bad curvature ($\sim H_o$). This stability criterion is identical to that obtained from energy theorem considerations for an $\mathscr{H}^{(2)}$ calculated in a frame rotating at rate $\Omega$.[13]

Figures 7 and 8 exhibit results of this analytical calculation and those obtained with FLORA. FLORA reproduces the frequencies (Fig. 7) calculated in Eq. (82) and the corresponding eigenfunctions (Fig. 8) to within a few percent for $1 \leq m \leq 6$, $\Omega\Delta t = 0.1$ and 40 radial grid points. The discrepancy of the eigenfrequencies near marginal stability is due to finite-differencing errors. There is also a small systematic discrepancy especially noticeable in $\mathrm{Re}\omega$, because $|\psi_w d\rho/d\psi| = 0.05\ \rho_o$ in the series of FLORA results displayed so that FLORA was not solving Bessel's equation (G is finite). The eigenfunctions exhibited in Fig. 8 were obtained with $d\rho/d\psi$ artificially suppressed except in the curvature-drive term where $d\rho/d\psi$ = const., and the correspondence of the FLORA results with the analytical calculation is better than 1% over most of the domain. The relative accuracy of FLORA's eigenfunctions appears to degrade only in the neighborhood of the endpoints (where both the numerical and the analytical solutions vanish).

## V. TANDEM MIRROR EQUILIBRIA

In this section we present the procedure used in FLORA to calculate finite-pressure paraxial equilibria. The perpendicular and parallel force balance relations were given earlier in Sec. II.A along with a number of constraints. We have opted for simple analytical models where possible. Let us say that both pressure components are separable functions of $\psi$ and B: $p_{\parallel,\perp}(\psi,B) = N(\psi)\ \hat{p}_{\parallel,\perp}(B)$, where

$$\hat{p}_{\parallel}(B) = a + bB + cB^2 + dB^4 \quad . \tag{84}$$

The perpendicular pressure is deduced from parallel pressure balance, Eq. (7) summed over species,

$$\hat{p}_{\perp}(B) = - B^2 \frac{\partial}{\partial B} \left(\frac{\hat{p}_{\parallel}}{B}\right) = a - cB^2 - 3dB^4 \ . \tag{85}$$

The pressures $p_{\perp}$ and $p_{\parallel}$ share the same $\psi$ profiles denoted as $N(\psi)$, which are composites of simple polynomials, Gaussians, and hyperbolic functions. Except for the purpose of studying sharp-boundary problems, the pressure profiles are spliced together smoothly so that they are twice-continuously differentiable with respect to $\psi$ and z. This ensures that equilibrium coefficients required in the stability equation are well behaved. Additional details are contained in the FLORA user's guide and source code listing.

The self-consistent magnetic field is calculated from the perpendicular pressure balance Eq. (2):

$$\frac{B^2}{2} + p_{\perp} = \frac{B_v^2}{2} \ , \tag{86}$$

where $B_v(z)$ is the axial magnetic field on axis due to external coils located outside the maximum $\psi$ surface. The field due to the external coils is assumed to have had sufficient time to penetrate conducting walls surrounding the plasma. The computation of $B_v(z)$ can be performed either numerically or analytically by superposition of simple current elements, e.g., finite-length solenoids. For a solenoid, the axial field is given by

$$B(z) = \frac{I}{2} \left\{ \frac{z_* + \Delta - z}{[a^2 + (z_* + \Delta - z)^2]^{1/2}} - \frac{z_* - \Delta - z}{[a^2 + (z_* - \Delta - z)^2]^{1/2}} \right\} , \tag{87}$$

where I is the current per unit length, $\Delta$ is the axial half-width of the solenoid, $z_*$ is the axial position of the solenoid center, and a is its radius. It has been convenient to express I for each solenoid in terms of the local vacuum magnetic field maxima. By varying parameters we have been able to accurately reproduce numerically calculated magnetic fields for quite complicated coil structures.

Equations (85) and (86) together yield a quadratic equation for $B^2$. Taking the physical solution (there is only one positive root), we obtain $r(\psi,z)$ (i.e., the explicit flux line radius) from

$$r^2 = 2\int_0^{\psi} d\psi'/B(\psi',z) \quad , \tag{88}$$

which is calculated numerically in general with z as a parameter. The curvature, $k = r_{zz}$, can be computed by differentiation under the integral sign (carried out analytically), followed by numerical evaluation of the integral.

An example of a model tandem mirror equilibrium is displayed in Fig. 9. This particular configuration has a choke magnetic field of 8 T and magnetic field peaks of 4 T in the anchor cell, wherein hot electrons with $\beta_{\perp e} = 2p_{\perp e}/B_v^2 = 0.1$ are magnetically confined. There is a central cell plasma with density $10^{12}$ cm$^{-3}$ and $\beta_\perp = 0.2$ relative to the central cell vacuum magnetic field. The $\beta$ values quoted will always be relative to the minimum of the vacuum magnetic field in the respective cell. There is a sloshing-ion plasma in the anchor with peak density $10^{12}$ cm$^{-3}$ and peak $\beta_\perp = 0.2$ relative to the vacuum magnetic field in the anchor midplane. The detailed profile shapes and parameters for this and other equilibria displayed subsequently in the paper are available in FLORA data files on the Magnetic Fusion Energy Computer Center Network.

We have constructed multiple-cell tandem mirror equilibria at finite plasma pressure in FLORA using this procedure. Parameters are selected to satisfy the constraints of positive $p_\perp$ and $p_\parallel$, validity of the paraxial approximation, firehose stability $Q > 0$, and the mirror mode condition (10). Attainable beta values, though fairly large (of order unity), are eventually limited by failure of the paraxial approximation or the mirror mode condition. The microstability condition (12) is often satisfied, but this is not a requirement.

The remaining equilibrium quantities required as coefficients in the stability equation are the FLR coefficients $\mathscr{X}$ and $\mathscr{Y}$ defined in Eqs. (15) and (16). These generally depend on the moments of the distribution functions and the electrostatic potential $\phi$. One can postulate distribution functions and then calculate the potential from the quasi-neutrality condition up to an arbitrary additive function of $\psi$.[14]

## VI. MHD STABILITY WITH HOT ELECTRONS

Hot electrons created by electron cyclotron heating or stacked in Astron rings[2] can depress the equilibrium magnetic field and provide a stabilizing magnetic well for a finite-beta core plasma. This MHD stabilization scheme has been analyzed theoretically,[39,40] but confirmation in experiments has been difficult to achieve. The same principle is being applied to several existing and proposed tandem mirror experiments (STM, TARA, and AXIM) with the goal of achieving an MHD-stable axisymmetric tandem mirror. A schematic of the concept is presented in Fig. 10. Hot electrons are mirror trapped in axisymmetric mirror cells at the ends of the tandem. The inside mirror peak may be a high-field magnetic choke coil, and a thermal barrier can be established by additional electron cyclotron heating in another mirror cell.[40] In this section we address the MHD stability of a simple tandem mirror equilibrium with hot electrons.

The well-digging effect of hot electrons can provide MHD stability to a core plasma that would otherwise be interchange unstable. When the drift frequency of the hot electrons much exceeds the characteristic MHD frequencies in the core plasma, the hot electrons become somewhat rigid in their response to MHD perturbations.[25,39,40] Solution of the Vlasov-Maxwell equations for compressible electromagnetic interchange modes indicates that the rigid-response approximation for the energetic electrons is qualitatively accurate, but stability is overestimated at larger values of the core beta.[39,40] The rigid-response model was adopted for the high-m MHD-fluid stability analysis in Ref. 25.

We also adopt a rigid-response model, and we limit investigation to incompressible perturbations. Furthermore, the core beta in the plug is assumed to satisfy $\beta_p < \mathcal{O}(2r_p/R_c)$, where $r_p$ is the plasma radius and $R_c$ is the radius of curvature. Above this $\beta_p$ the Nelson-Lee-Van Dam instability threshold is exceeded,[39,40] and the approximation of hot rigid electrons fails. Following this derivation is a presentation of results from FLORA illustrating that hot rigid electrons can stabilize MHD modes of arbitrary m number. Our two-dimensional study for general m including FLR effects differs in scope from Ref. 25 in which a one-dimensional high-m balloon equation in z was solved in the absence of FLR effects.

The prescription for incorporating rigid electrons has been given previously.[25,42-44] A separation is made between the plasma current and pressure, and the rigid-electron current and pressure. In equilibrium,

$$\nabla \times \underline{B} = \underline{J}_p + \underline{J}_e \tag{89}$$

and

$$(\underline{J}_p + \underline{J}_e) \times \underline{B} - \nabla \cdot (\underline{\underline{P}}_p + \underline{\underline{P}}_e) = 0 \quad . \tag{90}$$

Consider a low-beta, electrostatic ($\delta\underline{B} \equiv 0$), incompressible MHD perturbation. With hot non-responding electrons, the perturbed equation of motion is

$$- \rho \frac{d}{dt} \delta\underline{v} + \delta\underline{J}_p \times \underline{B} - \nabla \cdot \delta\underline{\underline{P}}_p = 0 \quad , \tag{91}$$

where $\delta$ indicates a perturbation quantity and the remaining quantities are evaluated at their equilibrium values. We introduce the displacement $\underline{\xi}$, assumed to be transverse and incompressible, and the velocity perturbation $\delta\underline{v} = d\underline{\xi}/dt$. It follows that $\delta n = - \underline{\xi} \cdot \nabla n$ and $\delta\underline{\underline{P}}_p = -\underline{\xi} \cdot \nabla \underline{\underline{P}}_p$. From Eq. (91)

$$\delta\underline{J}_{p\perp} = \left( -\rho \frac{d^2}{dt^2} \underline{\xi} + \underline{\xi} \cdot \nabla \underline{P}_p \right) \times \hat{b}/B \quad . \tag{92}$$

The quasineutrality condition is $\nabla \cdot \delta\underline{J}_p = 0$ (we assume that the hot-electron beta is finite, but that its density is negligible so that charge uncovering that could be caused by the plasma cannot occur), which we integrate along the field line with insulating boundary conditions $\hat{b}\cdot\delta\underline{J}_p = 0$ at the ends. Hence,

$$\int \frac{d\ell}{B}\, \nabla\cdot(\delta J_{p\parallel}\, \hat{b} + \delta\underline{J}_{p\perp}) = \int \frac{d\ell}{B}\, \nabla\cdot\delta\underline{J}_{p\perp} = 0$$

or

$$\int \frac{d\ell}{B}\, \nabla\cdot\, [(-\rho \frac{d^2}{dt^2}\, \underline{\xi} + \underline{\xi}\cdot\nabla\underline{\underline{P}}_p)\ x\ \frac{\hat{b}}{B}]$$

$$= im\int \frac{d\ell}{rB^2} \left\{\rho \frac{d^2}{dt^2}\, \xi - \xi \left[k \frac{\partial}{\partial r}(p_\perp + p_\parallel)_p - \frac{J_{\theta e}}{B} \frac{\partial}{\partial r}\, p_{\perp p}\right]\right\} = 0 \quad . \qquad (93)$$

In obtaining Eq. (93) we have made use of $m \gg 1$, $\nabla x(\hat{b}/B) = 2\hat{b}x(\hat{b}\cdot\nabla\hat{b})/B - (\underline{J}_p + \underline{J}_e)/B^2 \approx 2\hat{b}x(\hat{b}\cdot\nabla\hat{b})/B - \underline{J}_e/B^2$ for low plasma beta, $k = r_{zz}$, $\hat{b}\cdot\nabla x\nabla\cdot\delta\underline{\underline{P}}_p = \hat{b}\cdot\nabla x\ [\nabla\delta p_{\perp p} + \nabla\cdot(\delta p_\parallel - \delta p_\perp)_p\, \hat{b}\hat{b}] = -\hat{b}\cdot\nabla x\{[-\underline{\xi}\cdot\nabla(p_\parallel - p_\perp)_p]\ \hat{b}\cdot\nabla\hat{b}\}$, and the paraxial approximation. In the anchor, where $J_{\theta e} \gg J_{\theta p}$, $J_{\theta e} = -\partial B/\partial r$; and substitution of this in the right side of Eq. (93) illustrates explicitly the diamagnetic well-digging by the hot electrons. The result obtained in Eq. (93) agrees with the analyses of Refs. 25, 42, and 44, which were valid for arbitrary m and finite beta consistent with the Nelson-Lee-Van Dam condition. Thus, the change in the general stability equation (28) to accommodate hot rigid electrons is

$$-m^2 \frac{k}{rB} \frac{\partial}{\partial\psi}\, (p_\perp + p_\parallel)\ X \rightarrow [-m^2 \frac{k}{rB} \frac{\partial}{\partial\psi}(p_\perp + p_\parallel)_p + \frac{m^2}{B^2} \frac{\partial}{\partial\psi}\, p_{\perp e} \frac{\partial}{\partial\psi}\, p_{\perp p}]\ X \quad , \qquad (94)$$

where electron force balance in the plug determines $J_{\theta e} = r\partial p_{\perp e}/\partial\psi$. Equation (29) and the subsequently derived stability conditions are modified similarly.

An illustration of the stabilizing influence of hot electrons is given by the series of numerical studies in FLORA displayed in Figs. 11 and 12. Where the hot electron pressure profile decreases with respect to $\psi$, the self-consistent magnetic field increases and can stabilize a core plasma whose pressure profile is also decreasing, i.e., $(\partial p_{\perp e}/\partial\psi)(\partial p_{\perp p}/\partial\psi) > 0$ is stabilizing. Where $\partial p_{\perp e}/\partial\psi \geq 0$ and $k < 0$, the core plasma must be flat or hollow to ensure MHD stability on every field line. The results from FLORA shown in Figs. 11 and 12 demonstrate that complete MHD stabilization of a tandem mirror on every field line can be achieved with proper tailoring of the electron and core pressure profiles without recourse to FLR or a nearby conducting wall. Table I gives the peak beta values of the plasma in the central cell and plug, and the hot electron beta in the plug for representative stable and unstable cases. When the core plasma is unstable at finite pressure, the eigenmode balloons in the region that is most unstable locally as a result of bad curvature or rotation (Fig. 12e). An important aspect of hot-electron stabilization is that while the electrons dig a stabilizing well for the core plasma in the plug, they also increase the bad curvature in the midplane of the plug. Furthermore, maintaining consistency with the paraxial approximation may become difficult when the hot-electron beta becomes large over a limited axial extent.

A comprehensive study of axisymmetric tandem mirror stability at low frequency with hot rigid electrons, FLR effects, and a nearby conducting wall has been made with FLORA and reported in Ref. 41. The addition of FLR and a nearby conducting wall assist in stabilization and allow high central cell betas. A detailed description will be given elsewhere.

## VII. COLD PLASMA HALO STABILIZATION

In this section the stabilizing influence of a cold plasma surrounding a hot plasma core is examined analytically and numerically. The stabilization mechanism is line-tying of the cold plasma to a conducting end wall where $\underline{\xi} = 0$, which is communicated axially in the cold plasma along the field lines because of their resistance to bending at low beta and then radially inward to the hot plasma by FLR effects which tend to make the displacement rigid. Line tying at the end walls in the cold plasma depends on good electrical conduction between the halo and the end wall.[45-47] This may require an electron-emitting end wall intersecting the field lines holding the halo. The hot plasma core is assumed to be well insulated from the end wall so that a free-end boundary condition is appropriate $\partial\underline{\xi}/\partial z = 0$. The following analysis and computations address the influence of line tying on MHD stability.

The extension to general m of an m=1 analytical stability analysis[48] is presented here. The model for this analytical calculation is simplified and artificial, but illustrates the physics of stabilization by a conducting wall or a cold plasma halo. Consider a low-beta plasma with pressures and mass density whose radial profiles are Gaussians, $p_\perp + p_\parallel = p_o \exp(-r^2/r_p^2)$ and $\rho = \rho_o \exp(-r^2/r_p^2)$, and with bad curvature $k = -r/R_c^2$ where $R_c$ is the radius of curvature. Assume further that all coefficients in the stability equation and the transverse displacement $\xi$ are independent of z, so that Eq. (29) becomes

$$\frac{1}{r}\frac{\partial}{\partial r}\left(\rho T r^3 \frac{\partial}{\partial r}\xi\right) + (1 - m^2)\,\rho T \xi + r\omega^2 \xi \frac{\partial}{\partial r}\rho - 2m^2 k\,\xi \frac{\partial}{\partial r}\bar{p} = 0 \quad . \tag{95}$$

In an actual physical system, B and r must have some z dependence in order for k to be finite and negative. However, the z dependences can be quite weak, so that Eq. (95) is a reasonable approximation. The characteristic frequencies appearing in T are assumed to be constants.

We next assume that a cold plasma halo establishes the boundary condition $\xi = 0$ at $z = \pm L$ for $r \geq r_h > r_p$. Because of the low beta, the eigenmodes are flutes and $\xi(r,z) = 0$ for $r \geq r_h$. For $r < r_h$, $\partial\xi/\partial z = 0$ at $z = \pm L$ and hence for all z at low beta, which allows finite-amplitude eigenmodes in the hot-plasma case. With $\lambda \equiv r^2/r_p^2$ and $\eta \equiv \lambda \exp(-\lambda/2)\, \xi$, Eq. (95) becomes Whittaker's equation,[6,38]

$$\frac{d^2\eta}{d\sigma^2} + \left(-\frac{1}{4} + \frac{\kappa}{\lambda} + \frac{1 - m^2}{4\lambda^2}\right) \eta = 0 \tag{96a}$$

with Whittaker's function solutions

$$\eta = M_{\kappa,m/2}(\eta) = \eta^{(1+m)/2} \exp(-\eta/2)\, M\left(\frac{1 + m}{2} - \kappa,\ 1 + m,\ \eta\right) \tag{96b}$$

where $\kappa \equiv 1 - (\omega^2 + m^2\Gamma^2)/2T$, $\Gamma^2 \equiv -kp_o/r\rho_o$, and $M(1/2 + m/2 - \kappa,\ 1+m,\ \eta)$ is Kummer's function. The eigenvalue condition is determined by line tying in the halo so that $\eta = 0$ for $r = r_h$. Hence,

$$M(1/2 + m/2 - \kappa,\ 1 + m,\ r_h^2/r_p^2) = 0 \quad , \tag{97}$$

from which $\omega$ is obtained.

For the special case of $\Omega_2 = -\Omega_1$ so that $T = \omega^2 - m^2\Omega_1^2$, Eq. (97) leads to the dispersion relation

$$\omega^2 = \frac{m^2}{m_* + 1} (m_* \Omega_1^2 - \Gamma^2) \quad , \tag{98}$$

where $m_* = 2(\kappa-1)$ and $m_*$ for $m = 1,2$, and 3 is plotted as a function of $r_h^2/r_p^2$ in Fig. 13 as calculated from Eq. (97) and a numerical evaluation of Whittaker's function.[49] Equation (98) indicates complete stabilization by the combination of FLR and halo effects when $m_*\Omega_1^2 \geq \Gamma^2$. The eigenmode is not radially rigid for any m, and the stabilization increases for decreasing $r_h/r_p$ and increasing $\Omega_1$(Fig. 14). As m increases so does $m_*$, which further improves stability in Eq. (98). Thus, $m = 1$ is the most difficult mode to stabilize.

We have used FLORA to confirm these analytical results, to examine the influence of a cold plasma halo extending from $r_h$ to a wall at a much larger radius, and to investigate the effect of a weak z variation of the equilibrium (Fig. 14). The results from FLORA prove that the simple radial analytical model problem correctly predicts all the qualitative features of having an actual halo in a system with a weak z variation. There is fairly good quantitative agreement between the model calculation and FLORA on growth rates and eigenfunctions, although FLORA indicates growth rates that are systematically higher by ∿5% when there is a halo and weak z variation.

For $\Omega_2 \neq - \Omega_1$, the dispersion relation acquires an FLR gyroscopic term that is linear in $\omega$ and is always stabilizing. The extension of Eq. (98) to this case is

$$\omega = \frac{m m_*(\Omega_1 + \Omega_2)}{2(1 + m_*)} \pm \frac{m}{2(1 + m_*)} [m_*^2(\Omega_1 + \Omega_2)^2 - 4(1 + m_*)(m_*\Omega_1\Omega_2 + \Gamma^2)]^{1/2} ; \tag{99}$$

and $m_*$ remains determined by Eq. (97) and is plotted in Fig. 13 for m = 1,2, and 3. Numerical solution of the stability equation for spatially varying $\Omega_1$ and $\Omega_2$ or for more general pressure and density profiles is conveniently obtained in FLORA.

## VIII. DISCUSSION

This paper has addressed aspects of the low-frequency stability of axisymmetric systems in the paraxial limit including the effects of finite Larmor radius. The Lagrangian formulation of Ref. 12-14 has been used to derive the equation of motion for the linear incompressible transverse displacement of the perturbed field lines. This formulation is based on the solution of the Vlasov-Maxwell equations expanded in two small parameters, the inverse aspect ratio $R/L \ll 1$ and the ratio of the Larmor radius to the radial scale length $a/R \ll 1$. The stability equation derived in Sec. II describes MHD modes with frequencies much less than the cyclotron frequency. These modes are destabilized by bad curvature of the magnetic field lines or by rotation. We have also derived a statement of energy conservation for linear perturbations from which a sufficient condition for stability resulted.

We have solved a two-dimensional equation in flux coordinates $\psi$ and z for arbitrary azimuthal mode number m to assess the linear stability of axisymmetric equilibria. Analytical solutions for eigenfrequencies and eigenmodes are obtained in a number of special cases in Secs. IV, VI, and VII. In more general circumstances, the stability equation is integrated numerically as an initial-value problem with the FLORA computer code introduced here. The coefficients in the stability equation depend on the equilibrium profiles for the magnetic field, mass density, pressures, FLR coefficients, and ambipolar electric potential. These in turn depend on the distribution functions and a straightforward calculation of axisymmetric paraxial magnetostatic equilibrium at finite beta (Secs. II and V).

The analytical calculations presented in Secs. IV and VII illustrate many of the important physical characteristics of the stability equation and provide a basis of comparison for numerical integrations in FLORA. The basic instability drive mechanisms, unfavorable magnetic curvature and rotation, are emphasized in these examples. The stabilizing influences of gyroscopic ($\mathscr{X} \neq 0$) and quasi-elastic (if $\mathscr{Y} > 0$) effects are demonstrated. The stabilizing effects of a nearby lateral conducting wall and a cold-plasma halo that has good electrical contact with a conducting end wall are analyzed in Secs. IV and VII for low plasma beta.

The results of numerical calculations performed with FLORA have agreed with the analytical calculations and allowed us to address a more general class of equilibria where analytical solution of the stability equation is not always possible. The calculation of multiple-cell axisymmetric tandem mirror equilibria in FLORA is described in Sec. V. The stabilizing influence of hot "rigid" electrons is studied in Sec. VI, and the possibility of complete stabilization of a tandem mirror configuration to low-frequency incompressible MHD modes is demonstrated. The numerical examples reported here are intended to be illustrative; detailed parameter studies with FLORA will be described elsewhere.

In evaluating the implications for experiments and reactor designs of our stability calculations, it is important to remember their many limitations. Only paraxial systems have been analyzed. Weak FLR effects are incorporated, but there are no resonant particle effects. The low-frequency MHD modes analyzed are quasi-neutral and strictly incompressible because of the paraxial approximation. Compressional modes have higher frequencies in paraxial systems and are particularly important when considering the stability of finite-beta systems with hot non-rigid electrons.[25,39,40,50]

In the future, we will report on detailed stability studies of axisymmetric tandem mirror reactor designs and experiments. Preliminary results from FLORA on the MHD stability of an axisymmetric tandem mirror reactor design with hot electrons appear in Ref. 41. A study of Rayleigh-Taylor rotational stability including radial shear is in progress.[36] We have formulated the equation of motion describing the coupling of incompressible hot-electron precessional modes with shear Alfven waves and the resulting modification of FLORA in order to further study the stability of hot-electron stabilized tandems.[51] Finally, FLORA and supporting documentation are now available through the National Magnetic Fusion Computer Center in a public file.

## ACKNOWLEDGMENTS

We are pleased to acknowledge and thank L. D. Pearlstein for initially encouraging this study, numerous valuable suggestions, and assistance in the analysis. We are also grateful to D. A. D'Ippolito, D. R. Dobrott, J. H. Hammer, T. B. Kaiser, L. L. LoDestro, W. M. Nevins, and J. W. Van Dam, for many discussions, suggestions, and assistance.

This work was performed under the auspices of the U.S. Department of Energy by the Lawrence Livermore National Laboratory under contract number W-7405-ENG-48.

# REFERENCES

1. G. I. Dimov, V. V. Zakaidekov, and M. E. Kishinovskii, Fizika Plasmy 2, 597 (1976) [Soviet Phys. J. Plasma Phys. 2, 326 (1976)]; T. K. Fowler and B. G. Logan, Comments Plasma Physics Controlled Fusion 2, 167 (1977).
2. B. I. Cohen, ed., Status of Mirror Fusion Research 1980, Lawrence Livermore National Laboratory Report, UCAR 10049-80-Rev. 1 (1980) and references therein.
3. D. D. Ryutov and G. V. Stupakov, Fiz, Plazmy 4, 501 (1978) [Sov. J. Plasma Phys. 4, 278 (1978)]; R. H. Cohen, Comments Plasma Physics Controlled Fusion 4, 157 (1979).
4. M. N. Rosenbluth and C. L. Longmire, Ann. Phys. (New York) 1, 120 (1957).
5. K. A. Brueckner and K. M. Watson, Phys. Rev. 102, 19 (1956).
6. M. N. Rosenbluth, N. A. Krall, and N. Rostoker, Nucl. Fusion Suppl. Pt. 1, 143 (1962).
7. K. V. Roberts and J. B. Taylor, Phys. Rev. Lett. 8, 197 (1962).
8. M. N. Rosenbluth and A. Simon, Phys. Fluids 8, 1300 (1965).
9. A. MacMahon, Phys. Fluids 8, 1840 (1965).
10. L. D. Pearlstein and N. A. Krall, Phys. Fluids 9, 2231 (1966).
11. E. Bowers and M. G. Haines, Phys. Fluids 11, 2695 (1968) and 14, 165 (1971).
12. W. A. Newcomb, Nucl. Fusion Suppl. Pt. 2, 451 (1962).
13. W. A. Newcomb, Ann. Phys. (New York) 81, 231 (1973).
14. W. A. Newcomb, J. Plasma Phys. 26, 529 (1981).
15. M. Cotsaftis, Nucl. Fusion Suppl. Pt. 2, 447 (1962).
16. R. J. Wright, D. F. R. Pott, and M. G. Haines, Plasma Phys. 18, 1 (1976).
17. J. P. Freidberg and L. D. Pearlstein, Phys. Fluids 21, 1207 (1978).

18. L. D. Pearlstein and J. P. Freidberg, Phys. Fluids 21 1218 (1978).

19. W. A. Newcomb, Phys. Fluids 28, 505 (1985).

20. W. M. Tang and P. J. Catto, Phys. Fluids 24, 1314 (1981).

21. X. S. Lee and P. J. Catto, Phys. Fluids 24, 2010 (1981).

22. D. A. D'Ippolito and J. R. Myra, Phys. Fluids 24, 2265 (1981).

23. D. A. D'Ippolito, G. L. Francis, J. R. Myra, and W. M. Tang, Phys. Fluids 24, 2270 (1981).

24. D. A. D'Ippolito and B. Hafizi, Phys. Fluids 24, 2274 (1981).

25. D. A. D'Ippolito, J. R. Myra, and J. M. Ogden, Plasma Phys. 24, 707 (1982).

26. T. B. Kaiser and L. D. Pearlstein, Phys. Fluids 26, 3053 (1983).

27. T. B. Kaiser, W. M. Nevins, and L. D. Pearlstein, Phys. Fluids 26, 351 (1983).

28. M. W. Phillips and J. D. Callen, Phys. Fluids 27, 1733 (1984).

29. J. P. Freidberg and D. A. D'Ippolito, Phys. Fluids 26, 2664 (1983).

30. B. I. Cohen, S. P. Auerbach, J. A. Byers, and H. Weitzner, Phys. Fluids 23, 2529 (1980).

31. F. A. Haas and J. A. Wesson, Phys. Fluids 10, 2245 (1967).

32. D. A. D'Ippolito and J. R. Myra, Phys. Fluids 27, 2256 (1984).

33. H. L. Berk, M. N. Rosenbluth, H. V. Wong, and T. M. Antonsen, Jr., Phys. Fluids 27, 2705 (1984).

34. T. B. Kaiser and L. D. Pearlstein, Phys. Fluids 28, 1003 (1985).

35. B. Lehnert, Nucl. Fusion 11, 485 (1971).

36. J. H. Hammer, B. I. Cohen, and R. P. Freis, Bull. Amer. Phys. Soc. 29, 1301 (1984).

37. J. A. Byers and R. H. Cohen, submitted to Phys. Fluids.

38. T. D. Rognlien, Phys. Fluids 44, 3505 (1973).

39. D. B. Nelson, Phys. Fluids 23, 1850 (1980).

40. J. W. Van Dam and Y. C. Lee, in Proceedings of the Workshop on EBT Ring Physics (Oak Ridge National Laboratory, Oak Ridge, Tenn. 1979), p. 471.

41. D. Dobrott, D. D. Schnack, G. W. Shuy, H. Gurol, R. Freis, and B. Cohen, Bull. Amer. Phys. Soc. 29, 1375 (1984).

42. J. Johnson, R. Kulsrud, and K. Weimer, Plasma Phys. 11, 463 (1969).

43. G. Benford and W. A. Newcomb, Phys. Rev. Lett. 25, 1085 (1970).

44. D. B. Nelson and C. L. Hedrick, Nucl. Fusion 19, 283 (1979).

45. W. B. Kunkel and J. U. Guillory in Proc. of the Seventh International Conference on Ionized Gases, Belgrade, 1965, ed. B. Perovic and D. Tocsic (Gradjerinska Knjiga Publishing House, Belgrade, Yugoslavia, 1955) Vol. II, p. 702.

46. M. A. Lieberman and S. L. Wong, Plasma Phys. 19, 745 (1977).

47. D. Segal, M. Wickham, and N. Rynn, Phys. Fluids 25, 1485 (1982); A. W. Molvik, R. A. Breun, S. N. Golovato, N. Hershkowitz, B. McVey, R. S. Post, D. Smatlak, and L. Yujiri, Phys. Fluids 27, 2711 (1984).

48. L. D. Pearlstein, private communication.

49. E. Jahnke, F. Emde, and F. Lösch, Tables of Higher Functions, 6th Ed. (McGraw-Hill, New York, 1960) Ch. XI.

50. K. Tsang, X. S. Lee, B. HJafizi, and T. Antonsen, Phys. Fluids 27, 2511 (1984); K. T. Tsang and X. S. Lee, Phys. Rev. Lett. 53, 2094 (1984).

51. T. B. Kaiser and B. I. Cohen, private communication.

Table I. Plasma and hot-electron beta values for stable and unstable cases with no FLR.

| $\beta_{e\text{-}ring}$ | $\beta_{plug}$ | $\beta_{cent}$ | |
|---|---|---|---|
| 0.3 | 0.1 | 0.1 | Stable |
| 0.3 | 0.25 | 0.77 | Stable |
| 0.3 | 0.31 | 0.97 | Unstable |

# FIGURE CAPTIONS

Figure 1. Model two-cell axisymmetric tandem mirror equilibrium profiles as functions of $\psi$ and z for a plasma destabilized by bad magnetic curvature and axially sheared $\underline{E}\times\underline{B}$ rotation: (a) perpendicular pressure, (b) mass density $nm_i$, and (c) axially sheared rotation frequency $\Omega = \Omega_E (\Omega_E = 4 \times 10^2$ s$^{-1}$ or 0). The peak betas in the central cell and plug were very small ($\beta_\perp \sim 10^{-6}$). The magnetic field amplitude was 0.1 T in the central cell, 1 T at the mirror peaks, and 0.33 T in the midplane of the plug.

Figure 2. Growth rates and radial eigenfunctions for high-m MHD modes driven by curvature and rotation. (a) Infinite-m flute-averaged local MHD growth rate square $\bar{\gamma}^2$ as a function of the flux $\psi$ theoretically calculated (solid line) and observed in FLORA for m = 50 for the equilibrium exhibited in Fig. 1 with $\Omega = \Omega_E = 4 \times 10^2$ s$^{-1}$ throughout. (b) corresponding radial displacement $\xi = X/rB$ as a function of flux for m = 50 at various times in the FLORA computation.

Figure 3. MHD growth rates $\gamma$ for modes driven by curvature and axially sheared rotation as a function of (a) azimuthal mode number with $\Omega_a = 0$ and (b) relative shear in the anchor (a) and central cell (c), $1 - \Omega_a/\Omega_c$, for m = 50 and for plasma equilibria like that shown in Fig. 1. The dotted line indicates the theoretically predicted growth rate for infinite m.

Figure 4. Local growth rates and normal mode growth rates for curvature-driven interchange modes in a low-beta system. (a) $k^2 = -m^2e^2(1 + \bar{\gamma}^2/\omega^2)$ where $\bar{\gamma}$ is the local MHD growth rate as a function of the magnetic flux coordinate and $\omega$ is the eigenfrequency. (b) The quantity $1 - \omega^2/\gamma_o^2$ as a function of $1/m$ obtained in FLORA (data points) and with WKBJ theory (dashed line), where $\gamma_o^2$ is the maximum of $\bar{\gamma}^2$.

Figure 5. In (a-d), growth rates Im $\frac{\omega}{\Omega*}$ and frequencies Re $\frac{\omega}{\Omega*}$ for rotational eigenmodes as functions of $kv_A/\Omega*$ for $m = 1$, the lowest radial mode number $n = 0$, $\beta_o = 0.75$, and various rotation speeds $\alpha = -\Omega/\Omega*$. There was a conducting wall at 5 plasma radii from the axis. The radial eigenmode for $\alpha=2$ and $kv_A/\Omega* = 0.335$ as a function of radius is shown in (e). FLORA results are indicated as data points (x). The curves were taken from Ref. 17.

Figure 6. In (a-d), growth rates Im $\frac{\omega}{\Omega*}$ and frequencies Re $\frac{\omega}{\Omega*}$ for rotational eigenmodes as functions of $kV_A/\Omega*$ for $m = 2$, the lowest radial mode number $m = 0$, $\beta_o = 0.75$, and various $\alpha$. The wall radius was again at 5 plasma radii. The radial eigenmode for $\alpha = 2$ and $kv_A/\Omega* = 0.02$ as a function of radius is shown in (e). FLORA results (x) are superposed on the results of Ref. 17.

Figure 7. Frequencies and growth rates as a function of the magnitude of the FLR stabilization for m = 1 flute modes in an axially uniform plasma with pressures and density that are parabolic in radius. For $m = n = 1$ and $|\Delta\rho/\rho(o)| << 1$, the dispersion relation Eq. (82) can be written in the form $\omega = \Omega \pm i(\delta\Omega^2 - \gamma^2)^{1/2}$, where the FLR characteristic frequencies are $\Omega_{1,2} = \Omega \pm \delta\Omega$, $\gamma^2$ represents the destabilizing terms due to rotation and an artificially imposed gravity, and $\gamma/\Omega = 1.25$.

Figure 8. Radial eigenfunctions for the contravariant component of the displacement X as a function of radius for flute modes in an axially uniform plasma for m = 1 and 4: (a) X vs. r, (b) $X/J_1(r)$ vs. r, (c) X vs. r, and (d) $X/J_4(r)$, where $J_m(r)$ is the Bessel function.

Figure 9. Model axisymmetric tandem-mirror equilibrium profiles calculated in FLORA including stabilizing hot electrons. The peak central cell and anchor perpendicular betas (summed over species) are 0.2, and the hot-electron beta in the anchor cell is 0.1. There is no ambipolar electric field in this example. (a) the magnetic field B, (b) the curvature $k = r_{zz}$, (c) the mass density $\rho = nm_i$; (d) the perpendicular plasma pressure $p_\perp$, (e) the plasma parallel pressure $p_\parallel$, and (f) the hot electron perpendicular pressure $p_{\perp e}$ as functions of $\psi$ and z with nonuniform gridding.

Figure 10. Schematic of pressure and magnetic field profiles as a function of radius illustrating the stabilizing effect on the core plasma of the diamagnetic well due to hot electrons.

Figure 11. Typical equilibrium profiles as a function of $\psi$ and z computed in FLORA with nonuniform gridding: (a) the magnetic field B, (b) plasma perpendicular pressure $p_{\perp p}$, and (c) hot-electron perpendicular pressure $p_{\perp e}$ with a distant conducting wall. There was no ambipolar potential in these equilibria. The peak plasma beta was $\beta_{\perp p} = 0.1$ in both the plug and the central cell, and the hot-electron peak beta in the anchor was $\beta_{\perp e} = 0.3$.

Figure 12. Flute-averaged MHD growth rates squared as a function of flux and the modulus of the radial displacement $|\xi|$ at a reference position as a function of time calculated in FLORA. Without hot electrons, (a) $\overline{\gamma}^2$ vs. $\psi$ and (b) $|\xi|$ vs. time. With stabilizing hot electrons, $\overline{\gamma}^2$ vs. $\psi$ and (d) $|\xi|$ vs. time. FLR was suppressed and there was no ambipolar potential in these calculations. The peak beta of the plasma in the central cell and the midplane of the plug was $\beta_{\perp p} = 0.1$ relative to the vacuum magnetic field and the peak beta of the hot electrons was $\beta_{\perp c} = 0.3$. In (e) we display X vs. z for a ballooning unstable case with $\beta_{\perp p} = 0.2$ in both the central cell and the anchor, and no electron ring.

Figure 13. Theoretical eigenvalue relation $m_* \equiv 2(\kappa-1)$ as a function of $r_h^2/r_p^2$ for m = 1, 2, and 3, where $\kappa \equiv 1-(\omega^2 + m^2\Gamma^2)/2T$, $T = (\omega - m\Omega_1)\ (\omega - m\Omega_2)$, $r_h$ is the halo radius where $\xi = 0$, and $r_p$ is the e-folding radius for the Gaussian pressure and density profiles.

Figure 14. Squared growth rates normalized to $\Gamma^2 \equiv -k\ p_o/r\rho_o$ as functions of (a) $r_h^2/r_p$ and (b) $\Omega_1^2/\Gamma^2$. (c) Radial displacement $|\xi|$ as a function of $r^2/r_h^2$ for low-beta m=1 flute modes calculated in FLORA for $\Omega_1 = -\Omega_2 = 0.62\ \Gamma$ and with Gaussian density and pressure profiles. The solid lines in (a) and (b) are derived from the analytical dispersion relation Eq. (98). Code results with a conducting wall at $r_h$ and with no axial variation in (a) and (c) are indicated by (x) and with weak axial variation in (b) by (o). Data obtained with a halo beginning at $r_h$ and a conducting wall at 1.3 $r_h$ are denoted with a (+) in (a) and (c).

Cohen et al. - Figure 1

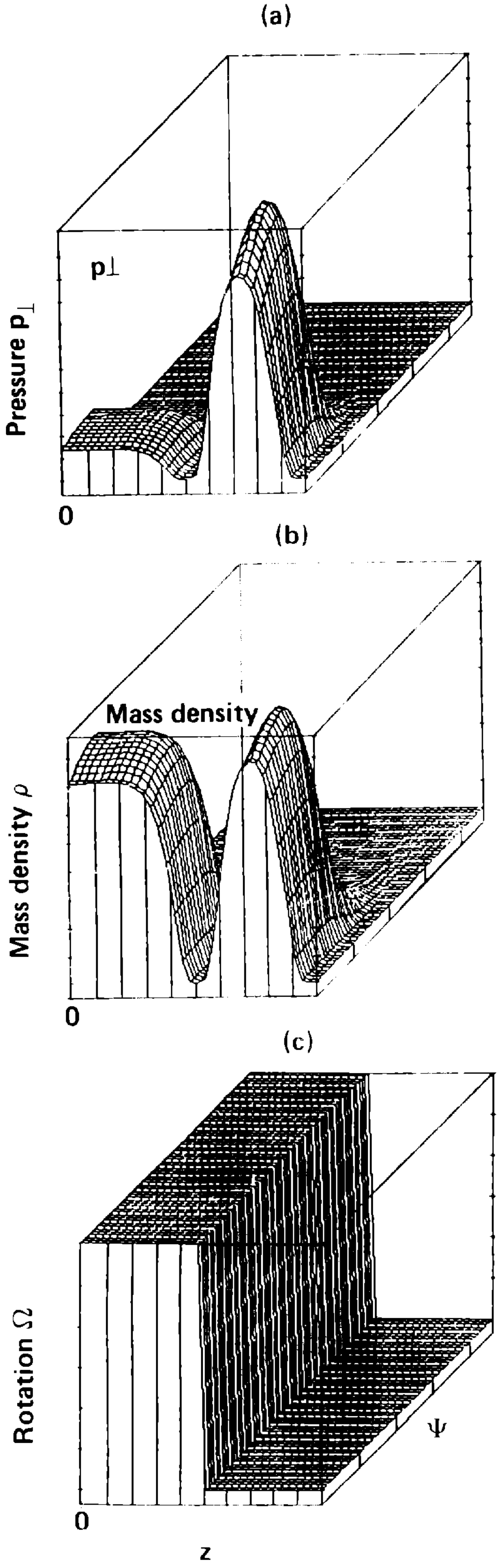

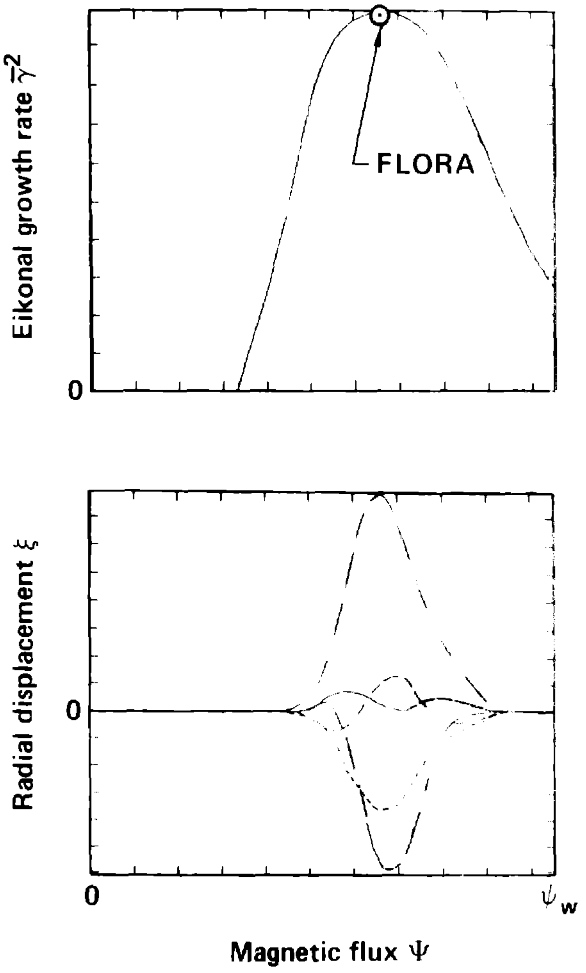
Eikonal growth rate $\bar{\gamma}^2$
FLORA
0
Radial displacement ξ
0
0
$\psi_w$
Magnetic flux Ψ

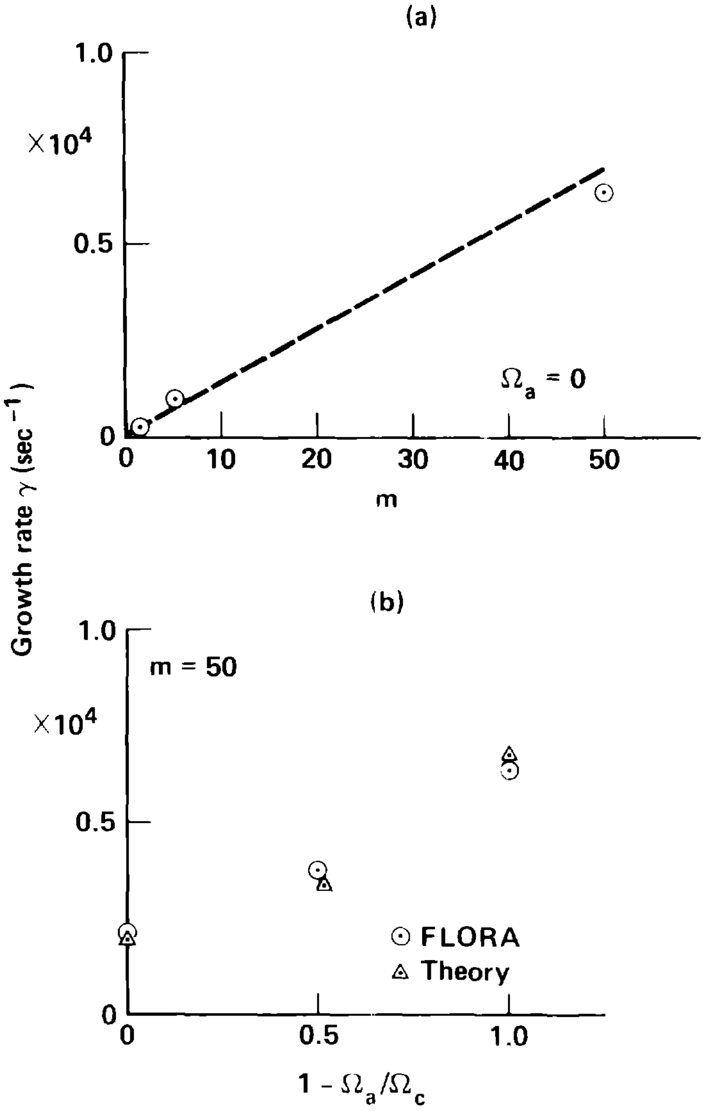
(a)
1.0
×10⁴
0.5
0
Growth rate γ (sec⁻¹)
Ω_a = 0
0
10
20
30
40
50
m
(b)
1.0
m = 50
×10⁴
0.5
0
⊙ FLORA
△ Theory
0
0.5
1.0
1 - Ω_a/Ω_c

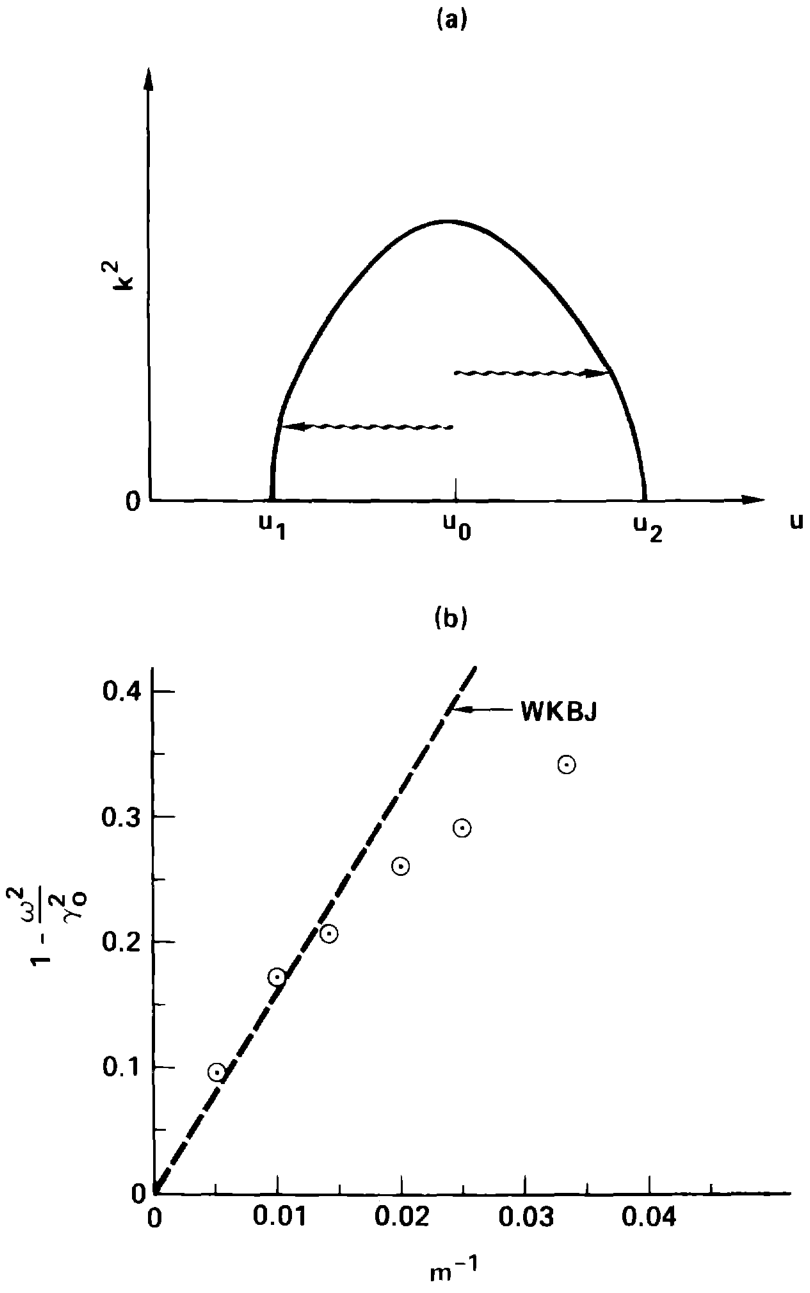
(a)
$k^2$
0
$u_1$
$u_0$
$u_2$
u
(b)
0.4
0.3
0.2
0.1
0
WKBJ
$1 - \frac{\omega^2}{\gamma_0^2}$
0
0.01
0.02
0.03
0.04
$m^{-1}$

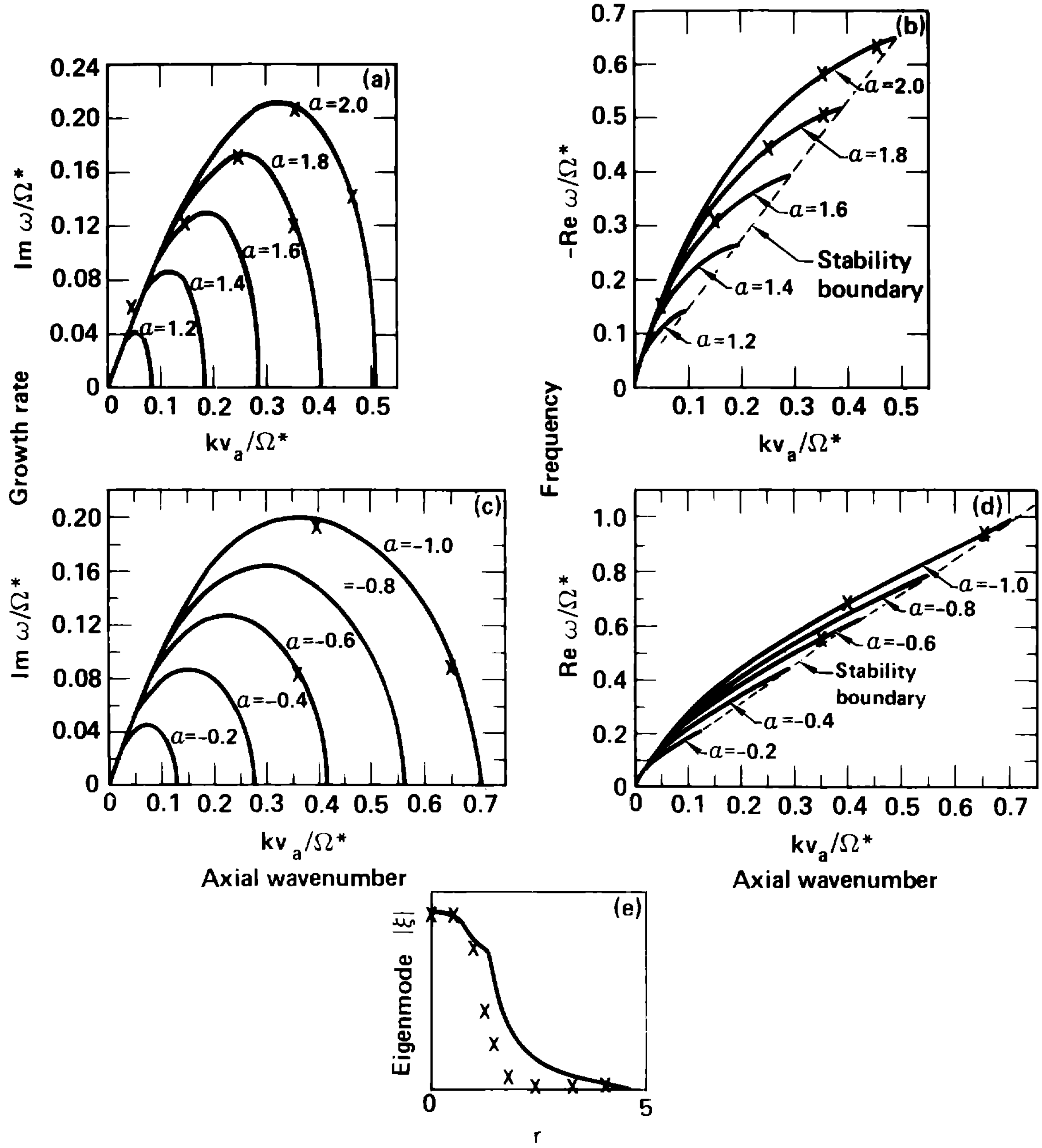
(a)
Growth rate
Im ω/Ω*
0.24
0.20
0.16
0.12
0.08
0.04
0
0 0.1 0.2 0.3 0.4 0.5
kv_a/Ω*
a=2.0
a=1.8
a=1.6
a=1.4
a=1.2
(b)
Frequency
-Re ω/Ω*
0.7
0.6
0.5
0.4
0.3
0.2
0.1
0
0.1 0.2 0.3 0.4 0.5
kv_a/Ω*
a=2.0
a=1.8
a=1.6
Stability boundary
a=1.4
a=1.2
(c)
Im ω/Ω*
0.20
0.16
0.12
0.08
0.04
0
0 0.1 0.2 0.3 0.4 0.5 0.6 0.7
kv_a/Ω*
Axial wavenumber
a=-1.0
=-0.8
a=-0.6
a=-0.4
a=-0.2
(d)
Re ω/Ω*
1.0
0.8
0.6
0.4
0.2
0
0 0.1 0.2 0.3 0.4 0.5 0.6 0.7
kv_a/Ω*
Axial wavenumber
a=-1.0
a=-0.8
a=-0.6
Stability boundary
a=-0.4
a=-0.2
(e)
Eigenmode |ξ|
0
5
r

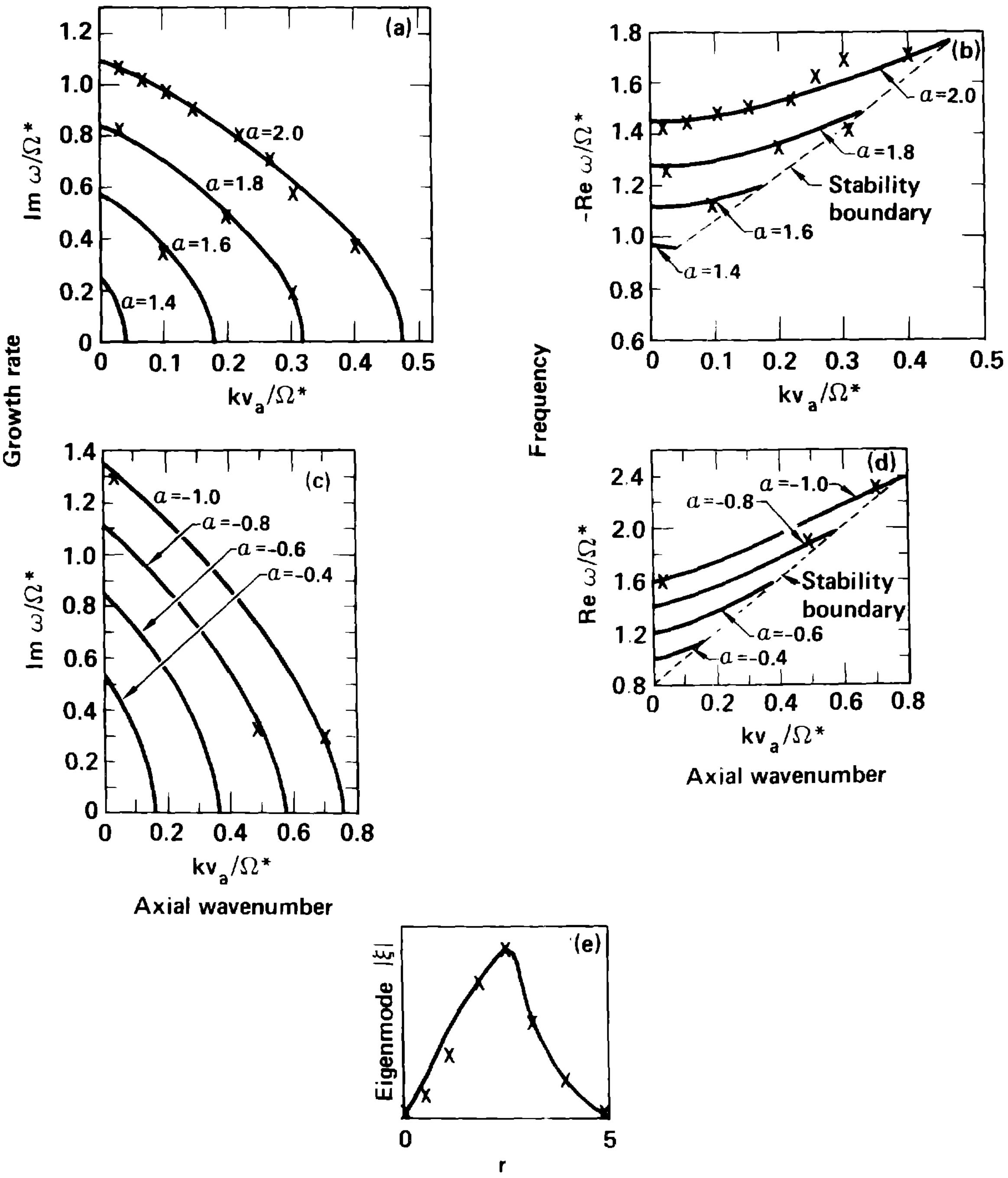
(a)
Growth rate
Im ω/Ω*
1.2
1.0
0.8
0.6
0.4
0.2
0
0.1
0.2
0.3
0.4
0.5
kv_a/Ω*
a=2.0
a=1.8
a=1.6
a=1.4
(b)
Frequency
-Re ω/Ω*
1.8
1.6
1.4
1.2
1.0
0.8
0.6
a=2.0
a=1.8
Stability boundary
a=1.6
a=1.4
(c)
Im ω/Ω*
1.4
a=-1.0
a=-0.8
a=-0.6
a=-0.4
Axial wavenumber
(d)
Re ω/Ω*
2.4
2.0
1.6
1.2
0.8
a=-1.0
a=-0.8
Stability boundary
a=-0.6
a=-0.4
(e)
Eigenmode |ξ|
0
5
r

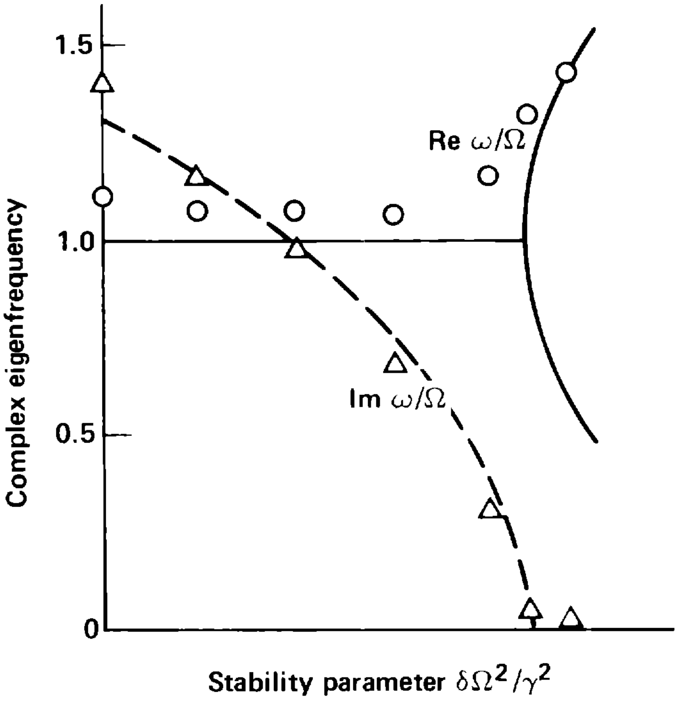
1.5
1.0
0.5
0
Complex eigenfrequency
Re $\omega/\Omega$
Im $\omega/\Omega$
Stability parameter $\delta\Omega^2/\gamma^2$

Cohen et al. - Figure 8

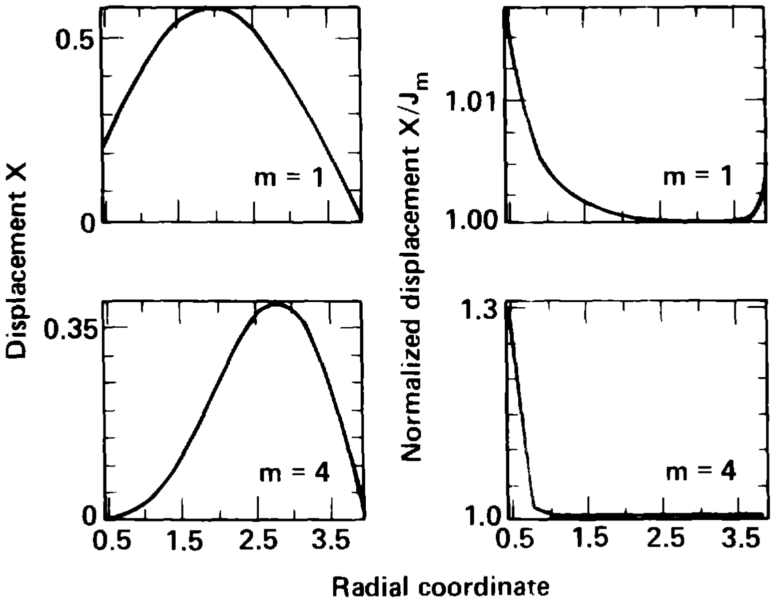

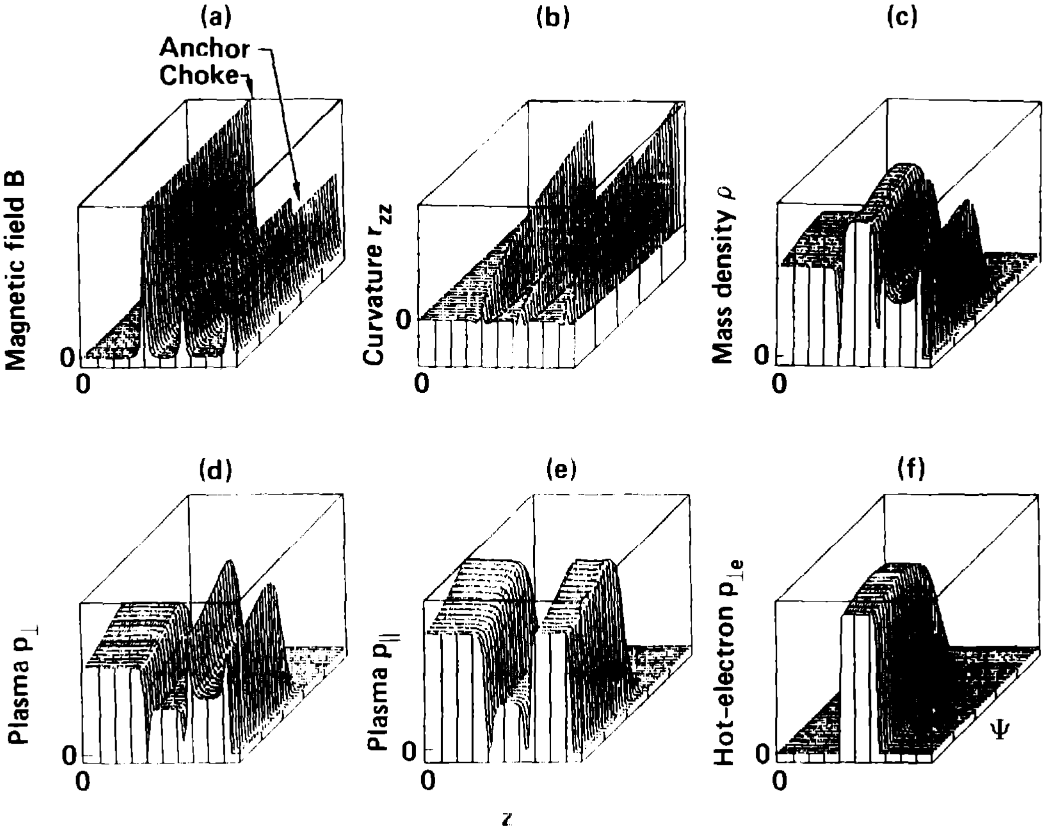
(a)
Anchor
Choke
Magnetic field B
0
0
(b)
Curvature $r_{zz}$
0
0
(c)
Mass density $\rho$
0
0
(d)
Plasma $p_\perp$
0
0
(e)
Plasma $p_\parallel$
0
0
(f)
Hot-electron $p_{\perp e}$
0
0
$\Psi$
z

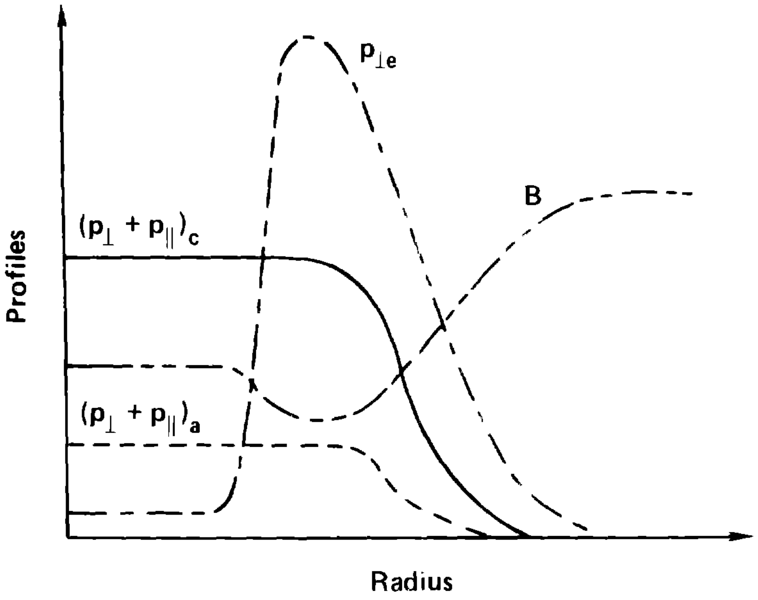
$p_{\perp e}$
B
$(p_{\perp} + p_{\parallel})_c$
$(p_{\perp} + p_{\parallel})_a$
Profiles
Radius

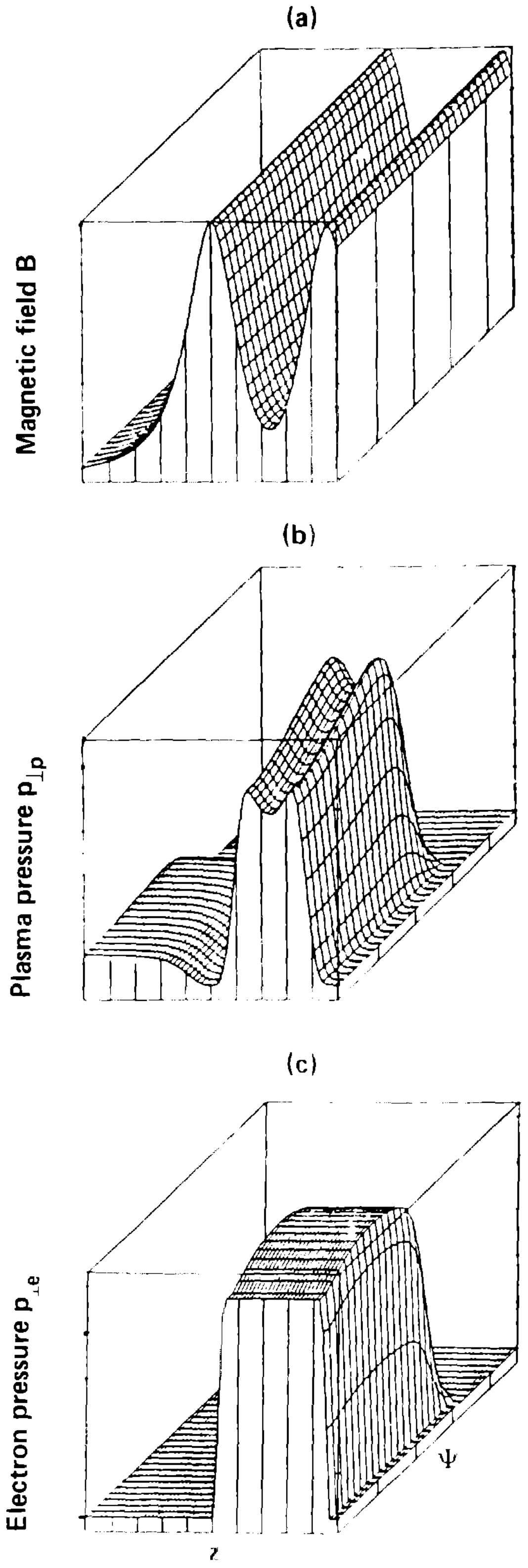
(a)
Magnetic field B
(b)
Plasma pressure p⊥p
(c)
Electron pressure p⊥e
z
Ψ

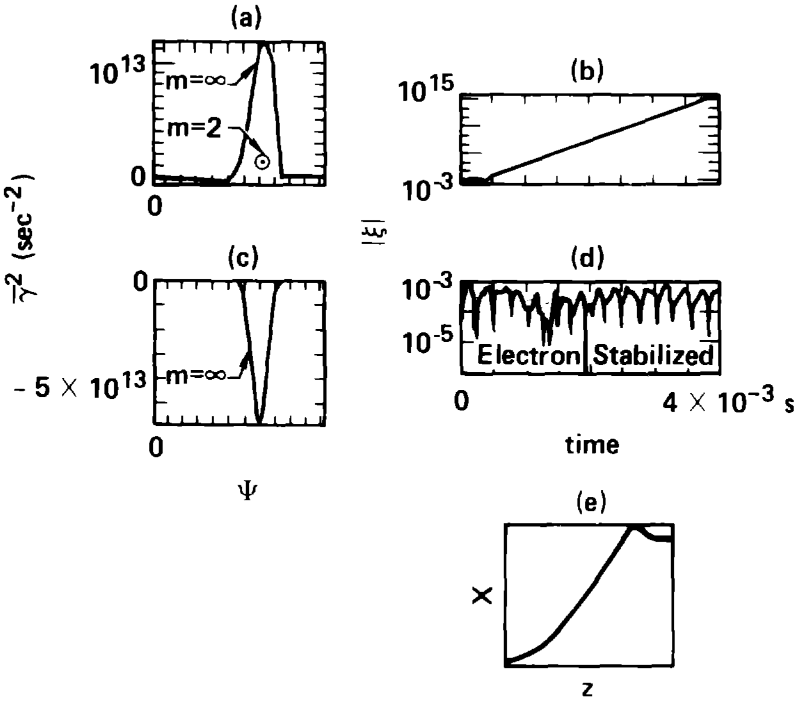
(a)
$10^{13}$
m=∞
m=2
0
0
(c)
0
$-5 \times 10^{13}$
m=∞
0
$\Psi$
$\bar{\gamma}^2$ (sec$^{-2}$)
(b)
$10^{15}$
$10^{-3}$
$|\xi|$
(d)
$10^{-3}$
$10^{-5}$
Electron Stabilized
0
$4 \times 10^{-3}$ s
time
(e)
X
z

Cohen et al. - Figure 13

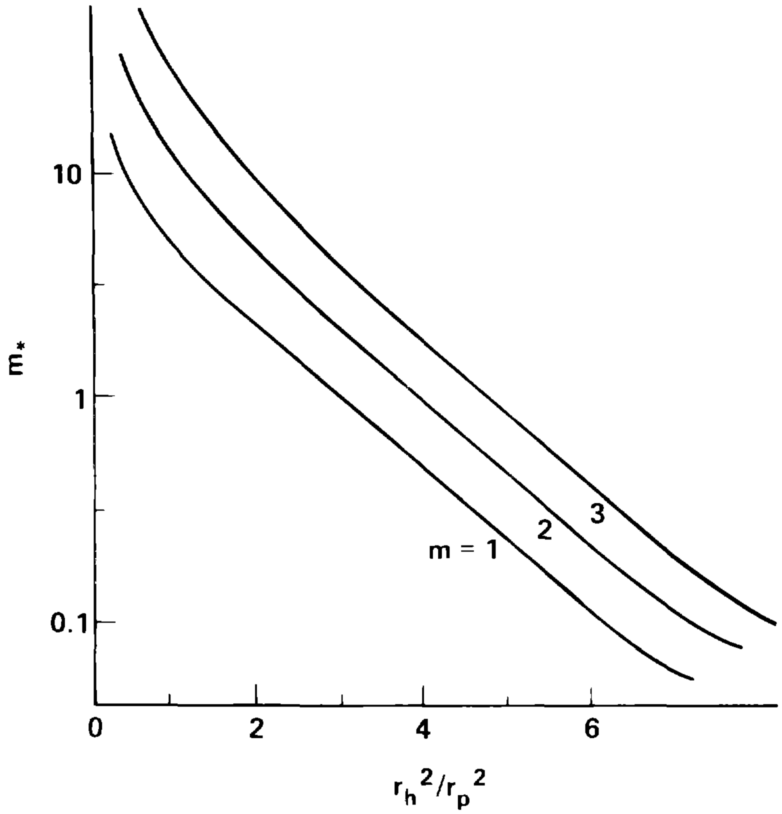

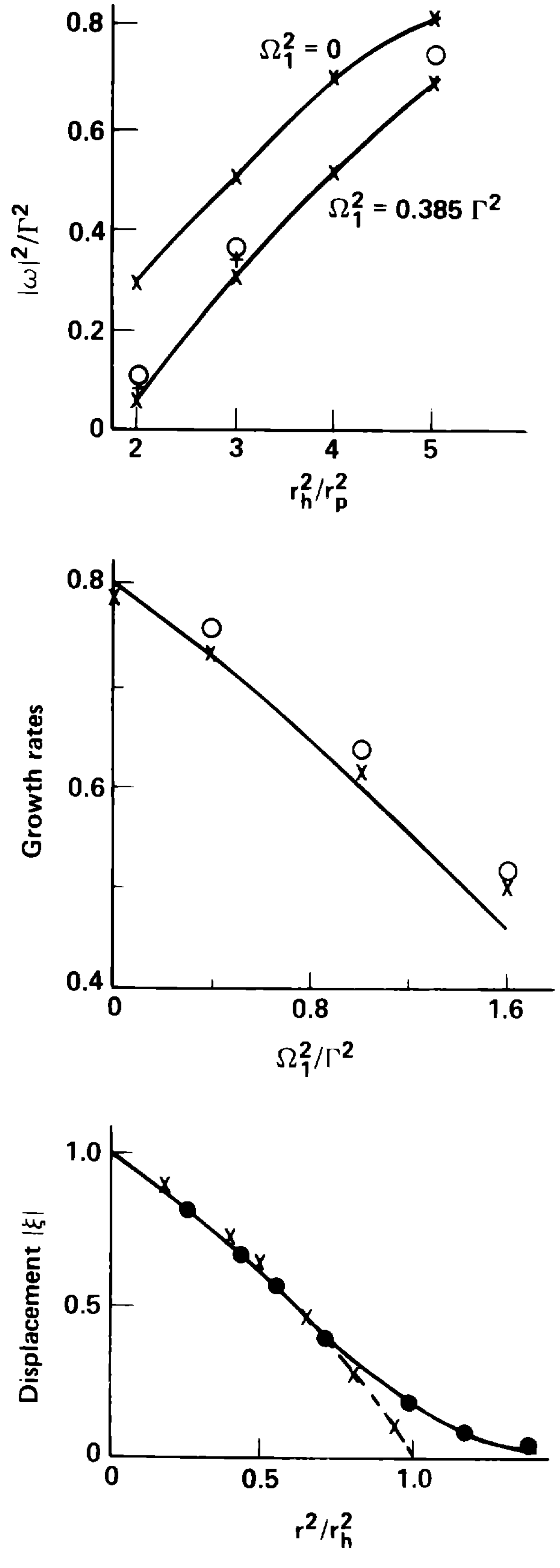Cohen et al. - Figure 14